NAVAL POSTGRADUATE SCHOOL

Monterey, California

THESIS

COMPUTER STUDIES OF SOUND PROPAGATION
IN A WEDGE-SHAPED OCEAN WITH
PENETRABLE BOTTOM
by

Demetrios Paliatsos

March 1989

Thesis Advisor: A. B. Coppens
Thesis Advisor: J. V. Sanders

REPORT DOCUMENTATION PAGE

1a REPORT SECURITY CLASSIFICATION UNCLASSIFIED	1b RESTRICTIVE MARKINGS
2a SECURITY CLASSIFICATION AUTHORITY	3 DISTRIBUTION / AVAILABILITY OF REPORT Approved for public release; distribution is unlimited
2b DECLASSIFICATION / DOWNGRADING SCHEDULE	
4 PERFORMING ORGANIZATION REPORT NUMBER(S)	5 MONITORING ORGANIZATION REPORT NUMBER(S)
6a NAME OF PERFORMING ORGANIZATION Naval Postgraduate School 6b OFFICE SYMBOL (If applicable) 52	7a NAME OF MONITORING ORGANIZATION Naval Postgraduate School
6c ADDRESS (City, State, and ZIP Code) Monterey, California 93943-5000	7b ADDRESS (City, State, and ZIP Code) Monterey, California 93943-5000
8a NAME OF FUNDING / SPONSORING ORGANIZATION 8b OFFICE SYMBOL (If applicable)	9 PROCUREMENT INSTRUMENT IDENTIFICATION NUMBER
8c ADDRESS (City, State, and ZIP Code)	10 SOURCE OF FUNDING NUMBERS PROGRAM ELEMENT NO. / PROJECT NO. / TASK NO / WORK UNIT ACCESSION NO

11 TITLE (Include Security Classification)
COMPUTER STUDIES OF SOUND PROPAGATION IN A WEDGE-SHAPED OCEAN WITH PENETRABLE BOTTOM

12 PERSONAL AUTHOR(S)
PALIATSOS, DEMETRIOS

13a TYPE OF REPORT	13b TIME COVERED	14 DATE OF REPORT (Year, Month, Day)	15 PAGE COUNT
Master's Thesis	FROM _____ TO _____	1989 March	84

16 SUPPLEMENTARY NOTATION
The views expressed in this thesis are those of the author and do not reflect the official policy or position of the Department of Defense or U.S. Govt.

17 COSATI CODES			18 SUBJECT TERMS (Continue on reverse if necessary and identify by block number)
FIELD	GROUP	SUB-GROUP	Wedge-Shaped ocean with penetrable bottom

19 ABSTRACT (Continue on reverse if necessary and identify by block number)
The sound distribution everywhere within a wedge-shaped fluid overlying either a slow or a fast bottom has been studied in this research. Collecting all the results of the previous works in this area and overviewing them has been the primary purpose. All the cases reported earlier have been studied, and some new ones have been added. The variation of the transition point distance with the shore distance as a variable was observed. In additional the isopressure patterns were verified by calculating the pressure amplitudes in axial direction.

20 DISTRIBUTION / AVAILABILITY OF ABSTRACT ☒ UNCLASSIFIED/UNLIMITED ☐ SAME AS RPT ☐ DTIC USERS	21 ABSTRACT SECURITY CLASSIFICATION UNCLASSIFIED
22a NAME OF RESPONSIBLE INDIVIDUAL Alan B. Coppens	22b TELEPHONE (Include Area Code) (408) 646-2116 22c OFFICE SYMBOL 61Cz

DD FORM 1473, 84 MAR 83 APR edition may be used until exhausted
All other editions are obsolete

Approved for public release; distribution is unlimited.

Computer Studies of Sound Propagation in a Wedge–shaped Ocean with Penetrable Bottom

by

Demetrios Paliatsos
Lieutenant, Hellenic Navy
B.S.,Hellenic Naval Academy,1979

Submitted in partial fulfillment of the
requirements for the degree of

MASTER OF SCIENCE IN ENGINEERING ACOUSTICS

from the

NAVAL POSTGRADUATE SCHOOL
March 1989

Author: _____
Demetrios Paliatsos

Approved By: _____
A. B. Coppens, Thesis Advisor

_____
J. V. Sanders, Thesis Advisor

_____
A. Atchley, Chairman,
Engineering Acoustics Academic Group

_____
Gordon Schacher, Dean,
Engineering and Sciences

ABSTRACT

The sound distribution everywhere within a wedge-shaped fluid overlying either a slow or a fast bottom has been studied. Collecting all the results of the previous works in this area and overviewing them has been the primary purpose. All the cases reported earlier have been studied, and some new ones have been added. The variation of the transition point distance with the shore distance as a variable was observed. In addition, the isopressure patterns were verified by calculating the pressure amplitudes in axial direction..

Keywords: Underwater acoustics; Three-dimensional underwater sound transmission; Ocean bottom slope; Acoustic fields; Computerized simulation; Shallow water;

Theses, (edc.)

TABLE OF CONTENTS

LIST OF TABLES

LIST OF FIGURES

LIST OF SYMBOLS

B = Wedge angle

G = Source angle measured upward from the bottom

D = Receiver angle measured upward from the bottom

R1 = Normalized source distance from the shore

R2 = Normalized receiver distance from the shore

Y0 = Normalized distance along the shore between the receiver and the source

$\frac{\rho_1}{\rho_2}$ = Ratio of medium density to the bottom density (density ratio)

$\frac{c_1}{c_2}$ = Ratio of speed of sound in the medium to the speed of sound in the bottom (speed of sound ratio)

$\frac{\alpha}{k_2}$ = Wave number in the bottom divided into the absorption in the bottom.

ACKNOWLEDGMENT

I would like to acknowledge the support of the Computer Center Department people for their support. Also I would like to thank my wife Polly and my children. Nikolas and Alexandros for their patience and support during these busy months.

I. INTRODUCTION

Sound propagation in an ocean with a sloping bottom has received considerable attention during recent years. Both theoreticians and experimentalists have been involved with this subject [Ref 1–19]. They have created a number of acoustic models to predict the sound field within a wedge shaped fluid overlying a penetrable or a rigid fluid bottom.

The acoustic field in a wedge shaped shallow water duct with ideal boundary conditions has been studied by Bradley and Hudimac[Ref. 1]. They have analyzed the case of an isospeed duct with one pressure release and one rigid surface. The theoretical analysis has been carried out in both image theory and normal mode theory. The relationship between the two has been explored for the case of a point source. The image sum was transformed via the Poisson transformation formula to the normal mode sum. The average acoustic field was then compared for the two approaches with good results. Also the two theoretical approaches were compared with experimental data from the west coast of Florida with fair results.

Kuznetsov [Ref 2] used the method of images to investigate the high–frequency field in a wedge. He showed that the method of images is better suited to the near field where, in addition to the normal modes of the discrete spectrum, the continuous spectrum plays a significant role. At distances from the source greater than ten times the layer thickness, the normal mode method works better. These results are based on the idealized model of a wave channel as a layer of water having plane boundaries over a fluid half space. The sound field in a wedge was described

as the sum of the image–source fields taking account of the coefficient of all reflections. A point source was used in a wedge with perfectly reflecting boundaries.

Kuznetsov in another study [Ref 3], has described the displacement of the normal modes which takes place in the vertical plane and causes each normal mode to emerge from the wedge into the half space at a certain distance, specific to the normal mode, from the vertex line of the wedge.

In 1975 Graves, Nagl, and Uberall [Ref 6] used the adiabatic range variation method, derived by Pierce and Milder [Ref 4,5], to perform an approximate separation into normal modes for the problem of an under–ocean channel with gradual range dependence of medium and boundaries. Their technique was illustrated by application to the isovelocity ocean wedge with rigid ocean floor, and compared with the exact solution of Bradley and Hudimac [Ref 1]. A good agreement was obtained for moderately large wedge angles, even when mode coupling was neglected.

In 1978, Coppens, Sanders, Ioannou and Kawamura [Ref 7], using computer models, predicted the acoustic pressure amplitude and phase in the upslope direction at the bottom of a wedge shaped fluid layer overlaying a fast fluid. The slopes of the wedges studied were about 2.4^{o} or 2.7^{o}. One of the models had infinite source distance while the other had the source at finite distance. The program outputs were compared with the experimental results using as variables the wave number and density. There were significant differences between the simple model and the experimental results because of the experimental limitations.

The results of shallow water acoustic experiments performed off the coast of Corpus Cristi, Texas, have been compared with theoretical computations by Rubano

(1980) [Ref 8]. A four–layer, fluid, normal–mode model was used to predict the group velocity dispersion and spatial amplitude distributions of the first and second modes. The results show good agreement between the measured and theoretical values.

In the same year (1980), comparison between experiment and theory was made by Jensen and Kuperman [Ref 9]. They used the parabolic equation model to study the modal cutoff during upslope propagation in a wedge–shaped ocean. They found that the cutoff is not abrupt but takes place over a finite distance which essentially provides an aperture for radiation of a beam into the bottom. Also the Gaussian representation of a point source in the PE model has given very good results in the presence of a bottom.

The modal cutoff during upslope propagation has also been studied by Pierce (1982)[Ref 10]. Since the adiabatic mode theory for upslope propagation in shallow water breaks down when the depth decreases to a critical value, he has used matched asymptotic expansion techniques to yield the acoustic pressure in the transition case. The derived characteristic critical–depth transition function give results which are in accord with computations reported by Jensen and Kuperman [Ref 9].

The same subject, the modal cutoff during upslope propagation, was studied by Arnold and Felsen using the image theory as a convenient starting point for collective treatment of ray fields and their conversion into local modes [Ref 11]. The numerical comparisons with the results of Jensen and Kuperman [Ref 9] showed good agreement.

The sound field in an absorbing fluid substrate underlying a wedge shaped fluid with higher sound speed has been studied by Coppens, Sanders, and Humphries in

1984 [Ref 12]. A Green's function extension of the image theory give the opportunity of doing all the calculations on a computer. Two different approximation methods were used. The end–point approximation gave solutions valid at great distances, and for absorptions representative of sedimentary materials. The saddle–point approximation has given good results under the apex. with no limit in the absorption.

In 1984 Baek [Ref 13] predicted the pressure amplitude and phase, everywhere within the wedge, in upslope direction, having a fast bottom. Three cases were studied, pressure release bottom, rigid bottom, and penetrable bottom.

In the same year (1984) LeSesne [Ref 14] studied and compared two computer programs using the method of images to determine the pressure and phase distribution. It was concluded that an infinite source is not approached until the source exceeds six hundred dump distances from the apex. All measurements were taken directly upslope with source distance equal to forty dump distances and the receiver on axis with the source. Comparison between the two programs show similar results.

One year later, in 1985 Borchardt [Ref 15] experimentally measured the sound pressure field everywhere within isospeed water overlying a sloping absorbing bottom. The experimental data were compared with the program developed by LeSesne [Ref 14]. The results showed that the program successfully predicts the on–axis upslope sound profile in a wedge–shaped medium. Particularly, measurements showed good agreement for $R2 \leq 10$, $\beta = 9.5^{0}$, $\rho_1/\rho_2 = 1.1$ and $Y0 \leq 50$. All the symbol definitions are given in the List of Symbols table.

A shallow water wedge with a slope up to 9^{0} has been experimentally studied by Tindle, Hobaek, and Muir in 1986 [Ref 16]. They presented experimental results

for downslope propagation and they defined the wedge modes as propagating normal modes with wavefronts which are curved into arcs of circles centered on the wedge apex.

In 1987 Kaswandi [Ref 17], studied the slow bottom case. The outputs were taken for the on–axis case with wedge angles of 6^{O}, 10^{O}, and 15^{O}. Three kinds of curves were observed, depending on the source distance.

At about the same time, a program with 3–D capabilities was used by Li [Ref 18] to predict the acoustic pressure distribution along the interface between a wedge–shaped fluid layer overlying fast or slow bottom. It was concluded that the major characteristics of the output graphs were insensitive to minor variations of the bottom.

In 1988 Doolittle and Tolstoy presented experimental data obtained in East Australian Continental Slope consistent with the theory of energetic horizontal refraction due to multiple reflections from a sloping bottom [Ref 19]. When viewed from above, the path of the ray appears to curve. As a result,the exact position of the source can be obtained from the details of this curvature.

The purpose of this research is to take all the outputs provided by the theses of Kaswandi and Li and try to build a physical understanding of the acoustic field from them. Also an attempt was made to obtain detailed comparisons between the DSLOW and 3LS4 programs for the same inputs,and to further investigate the transition point.

II. THEORY

The theoretical background of this research has been presented by Coppens, Sanders, Ioannnou and Kawamura [Ref 8]. What follows, in this chapter, is a summary of the most important points of the image theory and its application to the wedge–shaped ocean with penetrable bottom.

A. METHOD OF IMAGES

The assumptions that (1) the speed of sound is the same everywhere within the wedge and in the penetrable bottom and (2) the upper surface is a pressure release surface makes the method of images an appropriate approach for understanding the sound field in a wedge–shaped fluid. The sound paths are straight lines and the plane wave Rayleigh reflection coefficients, discussed by Kinsler, Frey, Coppens and Sanders [Ref 14], is a good approximation if the sound source is not too close to the bottom.

The geometry of the model used to predict the pressure amplitude and phase everywhere within the wedge is shown in Figure 1. For the wedge–shaped duct, cylindrical coordinates are used with the shore line as the axis (Figure 2). The images lie on a circle centered on the shore line.

In Figures 3 and 4, the relationship between the receiver and the nth image is shown. The angle θ_n of the nth image, measured from the bottom, is given by:

$$\theta_n = B\cdot(n-1)+G, \quad \text{for n odd}$$

$$\theta_n = B\cdot n - G \quad \text{for n even}$$

According to Sommerfeld's concept of an extended Riemann surface, the extension of the θ coordinate makes the number of images infinite. The total pressure and phase at any field point within the wedge is found by coherent summation of all spherical waves radiated from the infinite number of images. As the number of reflections associated with a given image increases, the pressure contribution of this image decreases. The infinite summation is approximated by taking the sum over N images where

$$n = \text{INTEGER}\ (180 / \beta)$$

Wedge angles of the form π/n have been used, where n is an integer, because diffraction terms were eliminated [Ref 2].

The distance R_n between the receiver and the nth image is given by:

$$R_n = \sqrt{R_1^2 + R_2^2 - 2 \cdot R_1 R_2 \cdot \cos(\theta_n - D) + Y_o^2}$$

for the upper group of images, and

$$R_n = \sqrt{R_1^2 + R_2^2 - 2 \cdot R_1 R_2 \cdot \cos(\theta_n + D) + Y_o^2}$$

for the lower group images.

The angle of incidence ϕ_{nm} of the n^{th} image on the m^{th} plane (described by the angle $m \cdot \beta$) is

$$\sin\phi_{nm} = \frac{[R_1 \cdot \sin(\theta_n - m\beta) + R_2 \cdot \sin(m\beta - D)]}{R_n}$$

The reflection coefficients $R(\theta_n)$ for the upper family of images and $R(\theta_n')$ for the lower family of images for a plane wave are

$$R(\theta_{nm}) = \frac{\frac{\rho_1 c_1}{\rho_2 c_2} - \Psi_{nm}}{\frac{\rho_1 c_1}{\rho_2 c_2} + \Psi_{nm}}$$

and

$$R(\theta_n'_m) = \frac{\frac{\rho_1 c_1}{\rho_2 c_2} - \Psi_{n'm}}{\frac{\rho_1 c_1}{\rho_2 c_2} + \Psi_{n'm}}$$

where

$$\Psi_{nm} = \frac{\sqrt{1 - (c_1/c_2)^2 \cos^2(\theta_{nm})}}{\sin(\theta_{nm})}$$

and

$$\Psi_{n'm} = \frac{\sqrt{1 - (c_1/c_2)^2 \cos^2(\theta_n'_m)}}{\sin(\theta_n'_m)}$$

The resulting complex pressure from the upper family of images is

$$Pu = \sum_{n=1}^{N} \frac{1}{R_n} \exp(-jkR_n) \cdot (-1)^{INT[(n+1)/2]} \prod_{m=0}^{M} R(\theta_{nm})$$

and the resulting complex pressure from the lower family of images is

$$P_I = \sum_{n=1}^{N} \frac{1}{R_n'} \exp(-jkR_n') \cdot (-1)^{INT[(n+1)/2]} \cdot \prod_{m=0}^{M} R(\theta_n'_m)$$

The sound field radiated by each image has been multiplied by the plane wave reflection coefficients corresponding to reflections encountered by the wave as it goes from the source to the field point.

The total complex pressure distribution P is the sum of the Pu and P_I:

$$P = Pu + P_I$$

B. NORMALIZATION

All distances are normalized in terms of the characteristic distance X_c. This is the distance measured from the apex along the wedge interface to the point at which the lowest mode attains cut off as shown in figure 5 [Ref 20].

The characteristic distance is defined as the distance from the shore at which the depth H is given by

$$k \cdot H = \frac{\pi}{2\sqrt{1 - \frac{c_1}{c_2}}}$$

For a fast bottom, the critical angle θ_c is

$$\frac{c_1}{c_2} = \cos\theta_c$$

since

$$kH = \frac{\pi}{2\sin\theta_c}$$

$$\tan\beta = \frac{H}{X}$$

$$k_1 X = \frac{\pi}{2\ \sin[\theta_c]\ \tan\beta}$$

The above formula gives the derivation of the characteristic distance X in the case of a fast bottom ($c_1 < c_2$). When slow bottom case is studied ($c_1 > c_2$), the characteristic distance can not be defined as above. A useful characteristic distance for slow bottom can be defined by inverting c_1/c_2

$$k\,X = \frac{\pi}{2\ \tan[\arccos(c_2/c_1)]\ \tan\beta}$$

The advantage of working with normalized distances is that the analysis is frequency independent.

A convenient normalization for the pressure amplitude is accomplished by multiplying the pressure amplitude at one meter from the source by the source distance (R1). This simplifies the interpretation considerably, especially in the case of large source–apex distance compared to X.

In the course of this research, a computer program has been created, the DEME program. This computer program provides an additional normalization. It normalizes all the pressure amplitudes to the first pressure measurement taken down from the surface. This slope normalization makes the shapes of the curves comparable, even if they have been obtained at different distances.

III. COMPUTER PROGRAMS

Two programs have been used for the purpose of this research. They are improved and more documented versions of the programs discussed by Kaswandi [Ref 17] and Li [Ref 18]. They use the same model but have different output displays.

A. PROGRAM DEME

In the beginning of the study reported in this thesis, the DSLOW program was obtained [Ref 17]. DSLOW is itself an improved version of the WEDGE and XSLOPE programs developed by Kawamura and Ioannou [Ref 7], and LeSesne [Ref 14] respectively.

DSLOW was developed to run on the IBM 3033 main frame of the Naval Postgraduate School. It uses the method of images to predict the pressure amplitude and phase within the wedge fluid overlying a slow bottom.

DEME, created from DSLOW, uses the same model to predict the pressure amplitude, and phase within the wedge fluid overlying a slow or a **fast** bottom.

The output is given in a table format or in a graph as shown in the Appendices. The DISSPLA graphics package and the EASYPLOT program, both of them available on the IBM 3033. have been used for the graphical outputs.

During this research, other versions of the original DEME program have been created with different outputs. All of them have been stored under Professor Coppens' account in the IBM 3033 in the Naval Postgraduate School.

The most important of these programs are:

1. **Program S** provides the pressure amplitude and phase at one specific point in the field. It must be used with the "Record on" command of the IBM 3033 for sending the results in a separate file.

2. **Program SDF** is a version of the DEME program which takes the input data from an input file and transfers the output to another file. With this technique the EASYPLOT program can be used to produce multiple graphs.

3. **Program PREC** uses double precision to reduce round–off errors. The outputs of PREC can be plotted with any other graphics software except DISSPLA. The DISSPLA package has some difficulty when applied to the output of double precision fortran programs.

4. **Program SLA1** generates graphs without the slope normalization.

B. PROGRAM 3LS4

This program gives alternate forms of data presentation. It uses the IBM 3033 and the DISSPLA package to generate a 3–D representation of the pressure amplitude distribution on the bottom or along any plane (defined by the D) within the wedge. It also provides a contour presentation of the same data.

Because of the large volume of numerical output, 3LS4 is ineffective for recognizing details.

An important limitation of the program is that the array containing the data must be initially dimensionalised to the exact size of the data file array. This information is normally passed from the data file during the program.

IV. DISCUSSION OF THE RESULTS

The DEME and 3LS4 programs have been created using the same model. Although they provide different output graphs they must agree at every point. The 3LS4 provides the pressure amplitude and phase on a plane defined by the receiver angle (D). The DEME program provides the pressure distribution and phase along a vertical line anywhere within the wedge. The programs were checked for both slow and fast bottoms. For the same input data, they gave the same outputs, as shown in Tables 1 and 2.

For a slow bottom ($c_1 > c_2$), three different types of curves of pressure amplitude as a function of depth have been observed. The same types of the curves have been noticed by Kaswandi [Ref 17] and are shown in Figure 6.

When the source distance (R1) is much smaller than the characteristic distance (X), the sound pressure is linearly dependent on receiver angle with the surface pressure equal to zero and the bottom pressure a maximum (R1 = 0.1) When R1 approximates X , the curve develops considerable curvature (R1 = 0.7).

When the source distance (R1) is slightly different from the characteristic distance X (R1 = 1.1), then a maximum and a minimum appear between the surface and the bottom.

When the source distance (R1) is greater than the characteristic distance (X) (R1 = 4), then the sound pressure has a maximum between the surface and the bottom. No minimum appears in this kind of the curves. When the value of R1 is much greater than X , several minima and maxima appear in the output curve (R1= 12).

Figure 7 shows the development of the second type of curve (R1 = 1.0) as the receiver distance is varied.

For the same input data (B = 10, G = 5, ρ_1/ρ_2 = 0.9), the fast bottom gave entirely different curves as shown in Figure 8. When the source distance (R1) is less than three times the characteristic distance (X), only the first mode is received everywhere within the wedge (R1 = 0.3, 1.1, 1.3). When R1 > 3, higher modes are excited and the curves are the superposition of several modes (R1 = 4).

A. TRANSITION POINT

For the slow bottom, when the source distance (R1) is about the same as the characteristic distance (X), the curve has a maximum and a minimum. The minimum is close to the bottom. A "transition point" has been defined by Kaswandi [Ref 17] as the receiver distance, for which the pressure above a minimum extrapolates to zero on the bottom.

Three examples are shown in the Figure 9 (R2 = 4.6, 6.4, 32). In all of them the pressure above the minimum can be extrapolated to zero pressure point at the bottom. The transition point phenomenon happens for source distances 1<R1<1.5 .

For 1 < R1 < 1.5 the shape of the pressure curves as the receiver distance (R2) is varied can be explained as follows: as the receiver is moved from (R2 = 1.5) to (R2 = 30) the minimum pressure amplitude decreases in magnitude and the first transition point is observed (Fig 7). With further increasing of R2, the minimum pressure amplitude of the curves decreases to a minimum value, and then increases arriving at a second transition point. For the receiver distances between the first and the second transition point, the extrapolation to zero pressure was observed to be above the bottom (Figure 7). With further increasing of R2, a third

transition point tries to form but, since the R2 is so large round–off error appears in the program output curve and the curve characteristics can not be easily recognized. In the figure 10, the locus of the two detectable transition points are shown as a function of R2 and the shore distance (Y0). Although it is not indicated in the figure 10 the points lie on circular arcs centered at the source. This may indicates that the transition point obeys the cylindrical spreading law.

The locus of the first and second transition points form curves which can be approximated by arcs of circles centered at the source (figure 10)

The transition point as a function of the source angle (G) was studied using the output data shown in Table 3. As the source angle changes, the transition point moves to a different receiver distance. Two different wedge angles were observed. The greater the source angle (G) , the smaller the receiver distance where the transition point occurs.

A possible explanation is that, by increasing the G the source is placed far from the angle value (D), where the minimum happens, so the absolute pressure values become smaller as the source angle increases. In figures 10a and 10b the pressure distribution of the bottom is shown for $G = 2.5^{O}$. In figures 10c and 10d the same case is represented with $G = 7.5^{O}$. These figures are generated with the program 3LS4 [Ref 18].

In the fast bottom case no transition point was observed. In Figure 11 the fast bottom case is shown when the shore distance (Y0) varies. This is the case of downslope propagation in a wedge–shaped fluid overlying a fast bottom. At the receiver's position (R2 = 32), as the shore distance is increasing ($0 < Y0 < 80$). only a curve like the first mode appears and no minimum is observed.

B. MORE CASES

For the fast bottom, when the source distance (R1) is bigger than 3, the higher modes start to appear. In Figure 12, R1 = 6 . As explained by Kaswandi [Ref 17] when R1 = 6 the first three modes are present. By increasing the source angle (G) the output curve changes because at some source positions some modes are reduced and some are amplified.

Some problems appear when the source is very close to the apex (R1 =0.1), as in Figure 13. The program seems to fail close to the bottom. It may be a round–off error of the computer because the absolute pressure values are very small. The round–off error is clearly shown in Figure 14, where it starts to appear when the source–receiver distance becomes too far. An attempt to eliminate this problem was made in the PREC program which was a double precision version of the DEME program. Also another try was made to run the DEME program in a 386 IBM compatible personal computer with 16–bit memory. Both of the tries gave smoother curves but they did not solve the problem.

C. SHORE DISTANCE AS A VARIABLE

Until now most studies were for on axis receiver positions (Y0 = 0). In the following discussion the shore distance (Y0) is the variable. In slow bottom three different source distances (R1) were studied (R1 = 0.5 , R1 = 1 and R1 = 5).

The first case is shown in Figure 15, where the source is close to the apex (R1= 0.5). At receiver position R2 = 4 , only the linear pressure curve is observed at all values of Y0 (0 < Y0 < 60).The effect of larger values of source and receiver distance (R1= 1, R2= 6) is shown in Figure 16. As Y0 increases, the curve forms a transition point at Y0 = 3 and then becomes a straight line at Y0 = 10.

Figure 17 illustrates the case when the source distance is greater than the characteristic distance (R1 = 5). Curves for four different values of Y0 are shown.

The same cases were studied also for the fast bottom. The outputs are shown in Figure 18 when the source distance is close to the apex(R1 = 0.5), in Figure 19 where R1 = 1 , and in Figure 20 where the R1 = 5. What is clear to be observed in these cases is the uncertainties, which are present in great distances. Also when R1> 3 the higher modes start to appear.

D. ANGULAR OUTPUTS

Examination of the contour plots revealed a general hyperbolic or elliptical pattern, therefore another try was made to understand the physical structure of the acoustic field by searching at some particular angle off the axis (arctan[Y0/R2]). As shown in Figure 21 output data were calculated every 10^{O} off the axis. The acoustic field was studied for two different source positions, for a small source distance(R1=0.5) and for a source distance greater than the characteristic distance (R1=10).

The bottom pressure distribution is shown in Figures 22 through 25. The slow bottom as well as the fast bottom has been studied. From the contour plots (Figures 23 and 25) it would appear that large values of the axis angle were more interesting, because the isopressure curves seem to be asymptotic to the axis angles.

In the Figures 26 through 28 , the pressure distribution along three different angles are shown for the slow bottom. The curves are unnormalized.

The fast bottom graphs for the same inputs are shown in Figures 29 through 34. Many different axis were studied from 0^{O} to 90^{O}. All the curves from 0^{O} up to 70^{O} seem to be the superposition of the first five modes (Figure 29, 30,and 31). From

75^{O} axis angle and for big receiver distances (R2) the graphs begin to have only the first mode. That means that the higher modes have been cut off. At 80^{O} all the outputs appear to be in the area where only the first mode is received. The R2 in all the graphs was varied between 10 and 60.

The slow bottom curves for any angle off the axis were observed to have uniform vertical pressure profiles as shown in Figures 26 through 28. The fast bottom curves for angles up to 80^{O} were observed to have complicated profiles as shown in Figures 29 through 32.

D. THE OTHER PARAMETERS

Variations of the other parameters such as the velocity ratio c_1/c_2 and the density ratio ρ_1/ρ_2 were studied by Kaswandi [Ref 17] for on axis measurements. The results showed no strong variation of parameters studied.

V. CONCLUSIONS AND RECOMMENDATIONS

In this research, the 3–D propagation of sound has been studied using the image theory. Two computer programs were used to provide the pressure amplitude distribution and phase everywhere within a wedge–shaped fluid overlying a fast or a slow bottom.

The DEME and the 3LS4 programs were checked for the same input data and they provided the same outputs for the same acoustic field points. After this check. it was concluded that the programs were consistent with each other.

The transition point, present only over the slow bottom, was studied at various places inside the wedge. It was found that all the curves could be approximated by concentric circular arcs, having the source at the center.

As the source angle (G) increases, it was concluded that the transition point distance decreases as it is shown in Table 3 .

When the source position is $1.1 < R1 < 1.5$ then two transition point curves were formed. Sometimes it was possible to have also a third one, if the computer could work with very small numbers (16 or 32 bit Bus).

The off axis data were taken along many angular axes. The slow and the fast bottom were studied for the same angles of axis. The slow bottom data showed very small variation of the pressure amplitude values as the receiver distance was increased. The fast bottom curves showed very clearly the wave guide cutoff phenomenon. In all the axis angles up to 80^{o} the curves were observed to be irregular with many variations and unique for each R2. At the angle of 80^{o} or more, no major variations were observed as the R2 was increased. This observation

was found to be consistent with the contour plot output data taken from the 3LS1 program.

This research was another phenomenological theoretical step toward elucidating features of the wedge problem. Some experimental data must be compared with the two programs DEME and 3LS4 to have some confirmation of the programs capabilities. The most interesting case seemed to be the slow bottom case.

Current thoughts [Ref 23] suggest that these features can be studied from another point of view based on a collection of dipoles. The source and its first image form a dipole as do other associated pairs of images (Figure 1). If all these pairs of images are considered, then the field can be considered to be formed from the near cancellation of equivalent dipole pairs lying at slightly different distances from the receiver.

APPENDIX A

TABLE 1

CONSISTENCY OF THE DEME AND 3LS4 PROGRAMS (SLOW BOTTOM)

$B = 10^{O}$, $G = 5^{O}$, Y0 = 50, R1 = 40, R2 = 10, $\rho 1/\rho 2 = 0.9$, c1/c2 = 2

RECEIVER ANGLE D	OUTCOMING PRESSURE AMPLITUDE	
	DEME	3LS4
00	0.5073	0.50728
01	0.8683	0.86828
02	1.4251	1.42509
03	1.8969	1.89691
07	1.8491	1.84912
10	0.0000	0.00000

TABLE 2

CONSISTENCY OF THE DEME AND 3LS4 PROGRAMS (FAST BOTTOM)

$B = 10^{O}$, $G = 5^{O}$, R1 = 40, R2 = 35, $\rho_1/\rho_2 = 0.9$, $C_1/C_2 = 0.9$

REC.ANGLE	SHORE DIST.	PRESSURE AMPLITUDE OUTPUT	
D	Y0	DEME	3LS4
00	00	9.5446	9.54476
00	30	2.5776	2.57740
00	50	3.2210	3.22089

TABLE 3

TRANSITION POINT AS A FUNCTION OF SOURCE ANGLE (G)

$\rho_1/\rho_2 = 0.8,\ C_1/C_2 = 1.1$

WEDGE ANGLE (B)	SOURCE ANGLE (G)	SOURCE DIST.(R1)	RECEIVER DIST.(R2)
10^0	2.5^0	1.0	33.0
10^0	5.0^0	1.0	24.0
10^0	7.5^0	1.0	22.0
06^0	1.5^0	1.3	5.9
06^0	3.0^0	1.3	5.7
06^0	4.5^0	1.3	5.4

APPENDIX B

FIGURES

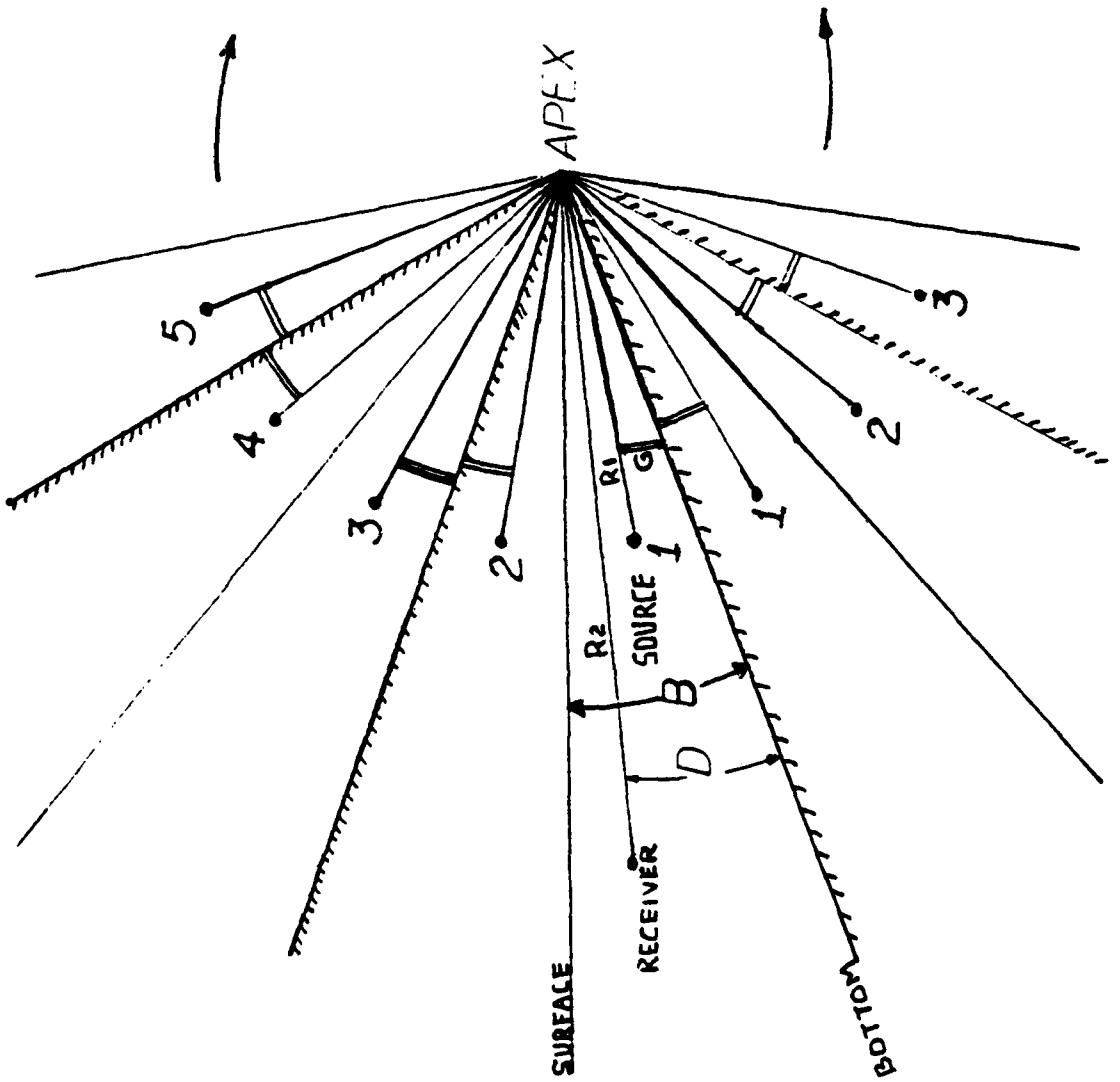

Figure 1 Image Structure for a wedge–shaped duct

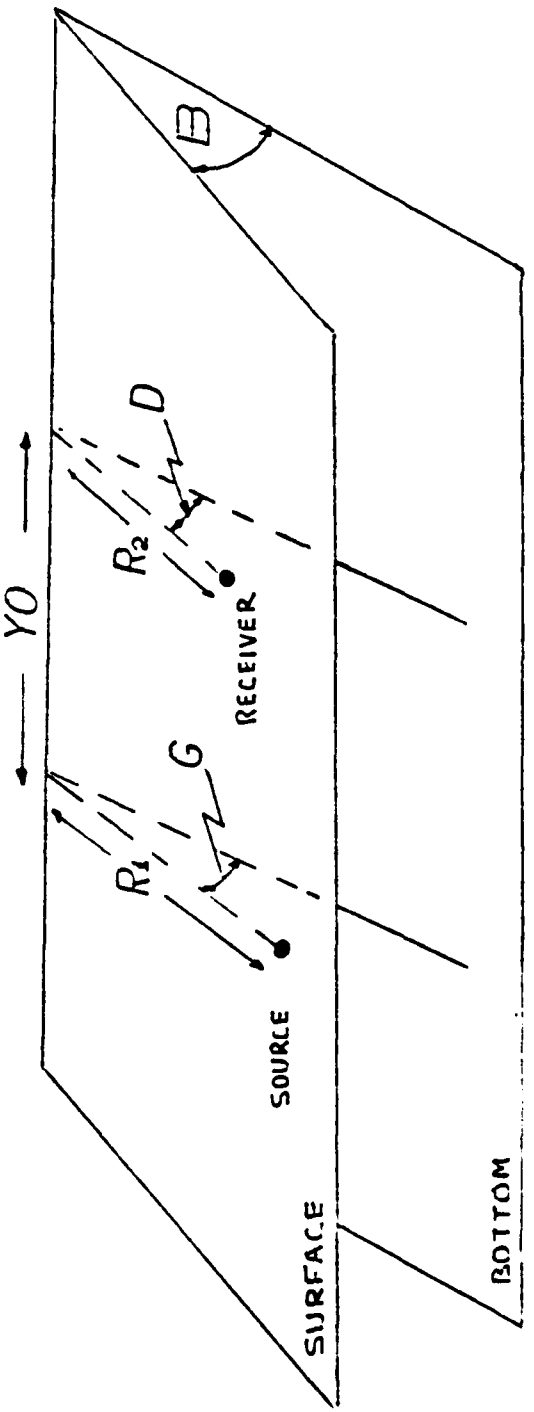

Figure 2. Definition of Source and Receiver Parameters

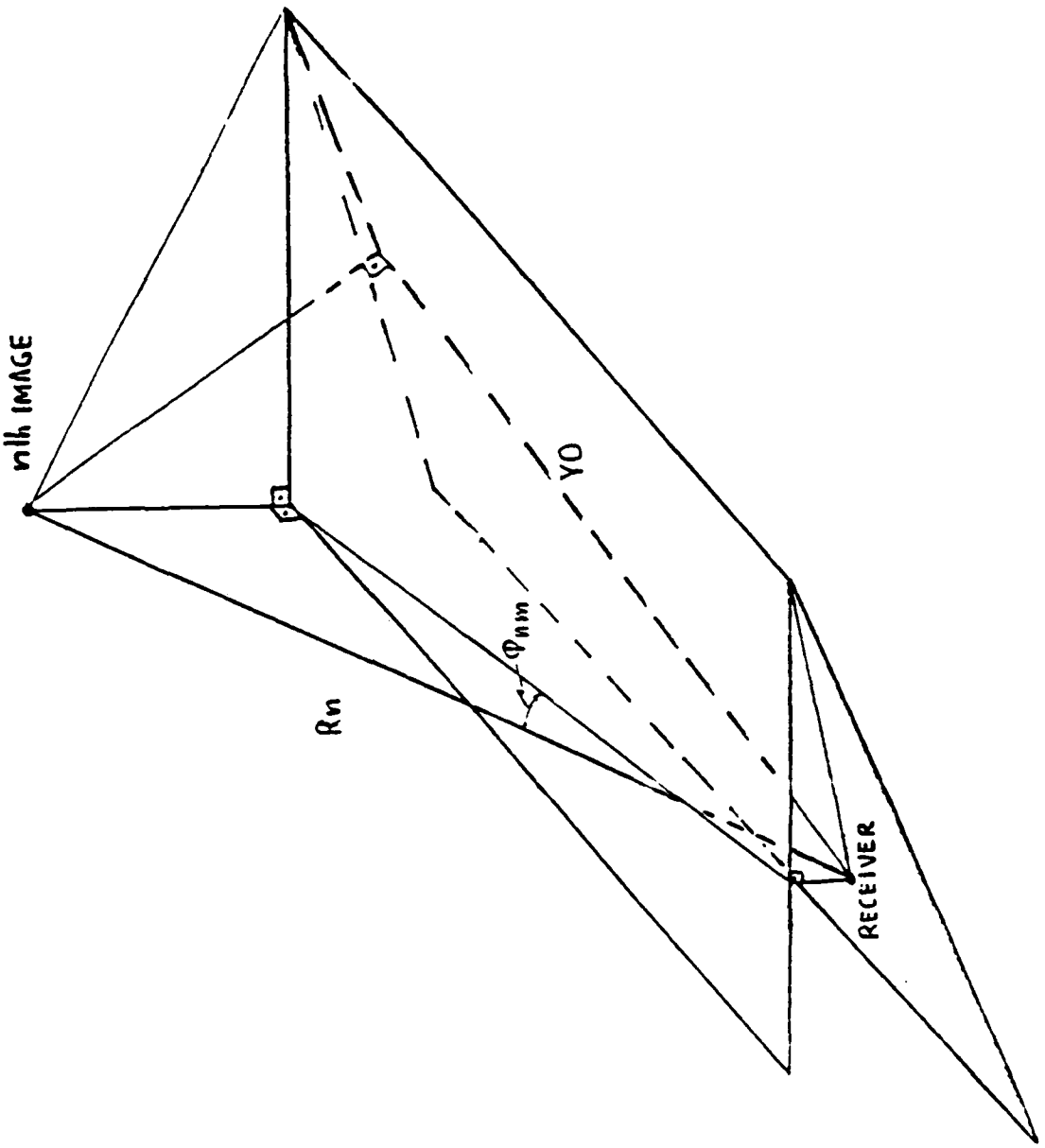

Figure 3. Range and Angle at Bottom of the n^{th} Image.

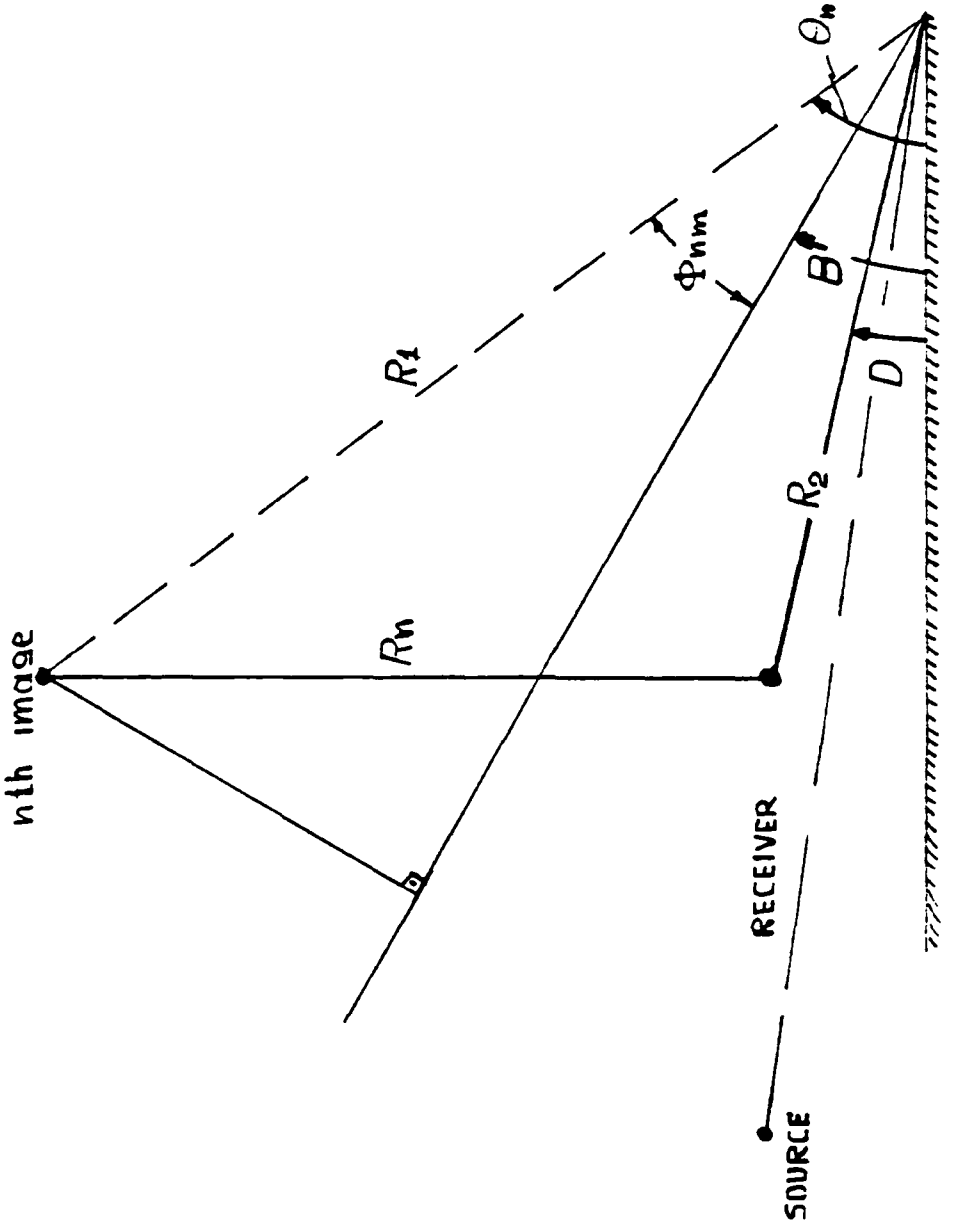

Figure 4. Geometry of the Nth Image and the Receiver projected onto a Plane

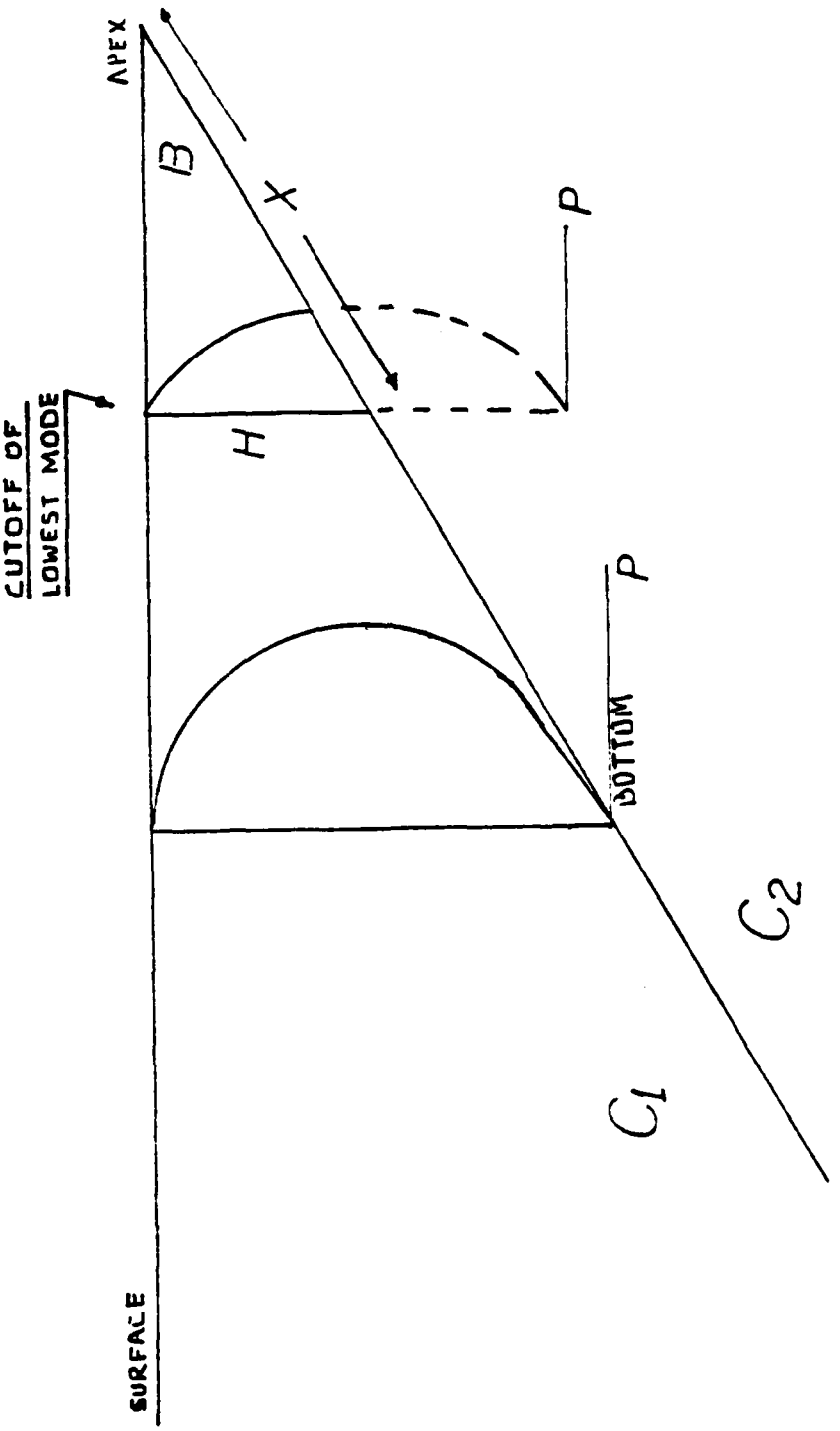

Figure 5. **Characteristic Distance**

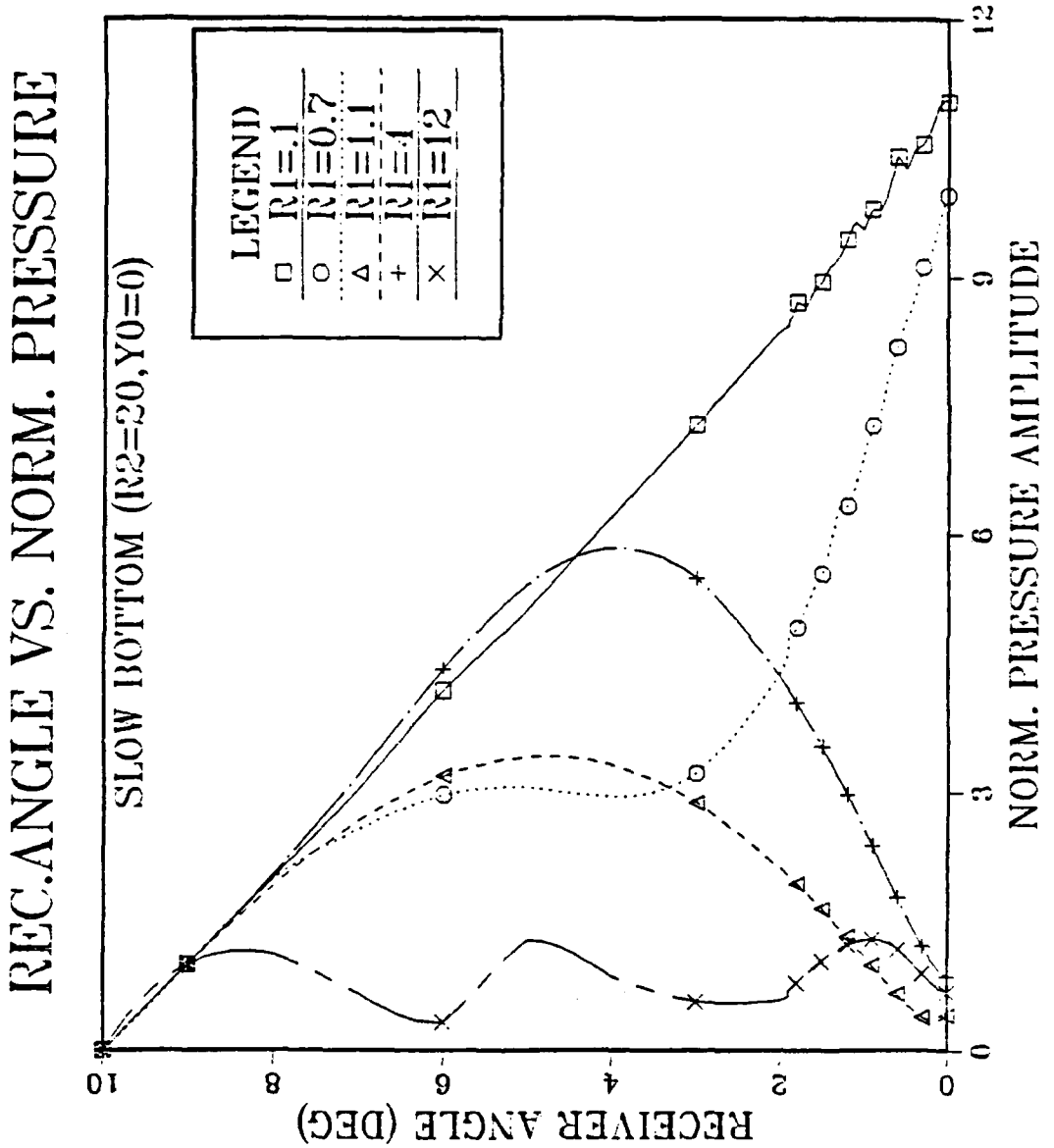

Figure 6. **Pressure Amplitude at R2=20 and Y0=0 for various R1 over a Slow Bottom. ρ_1/ρ_2 = .9, c_1/c_2 = 1.1 . (For clarity only every 5th computation shown)**

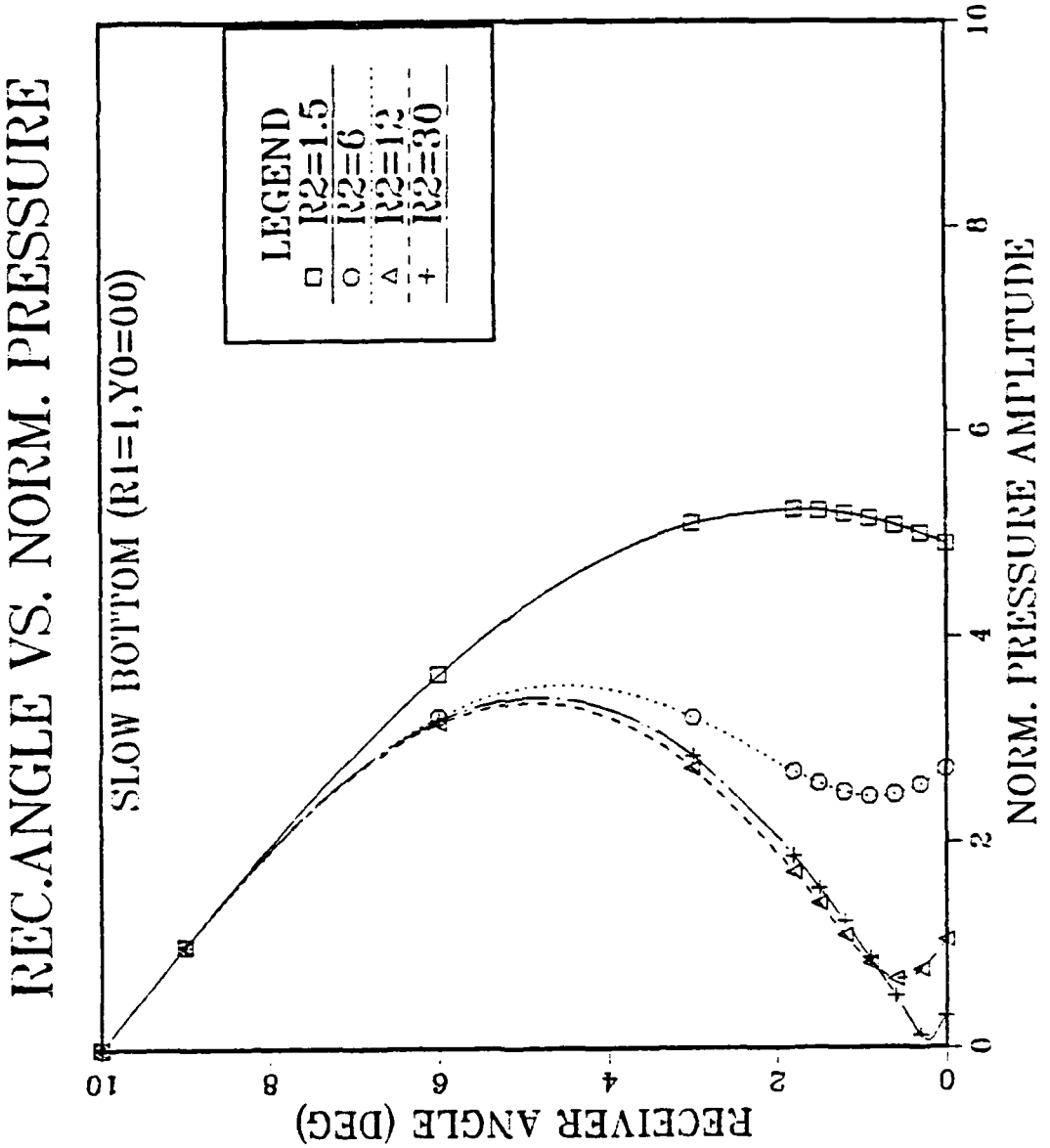

Figure 7. **Pressure Amplitude at R1=1 for Various R2 over a Slow Bottom ρ_1/ρ_2 = .9, c_1/c_2= 1.1 .(For clarity only every 5th computation shown)**

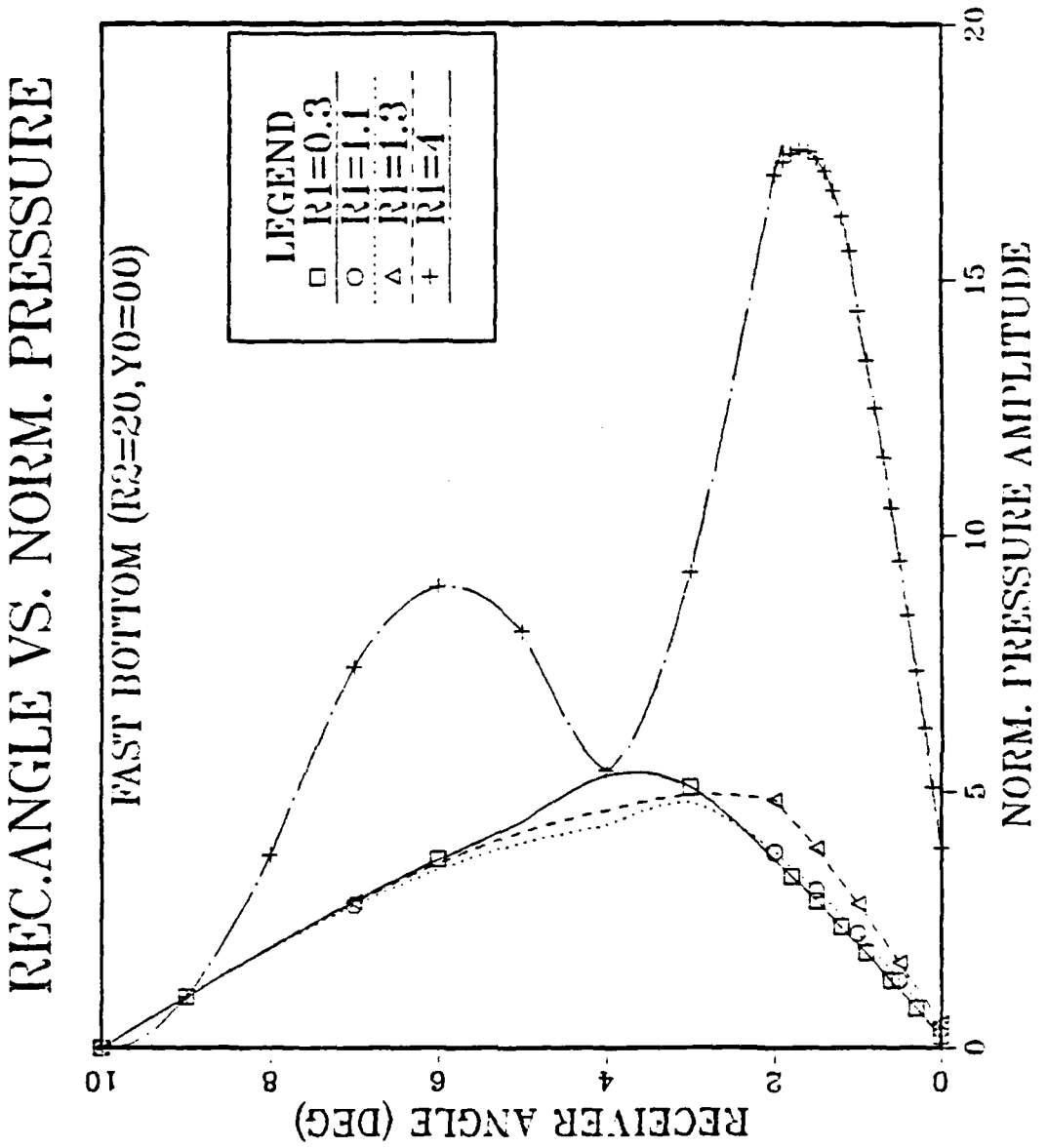

Figure 8. **Pressure Amplitude at R2=20, Y0=0 for Various R1 over a Fast Bottom. ρ_1 ρ_2 = 0.9, c_1/c_2 =.9192 .(For clarity only every 5th computation shown)**

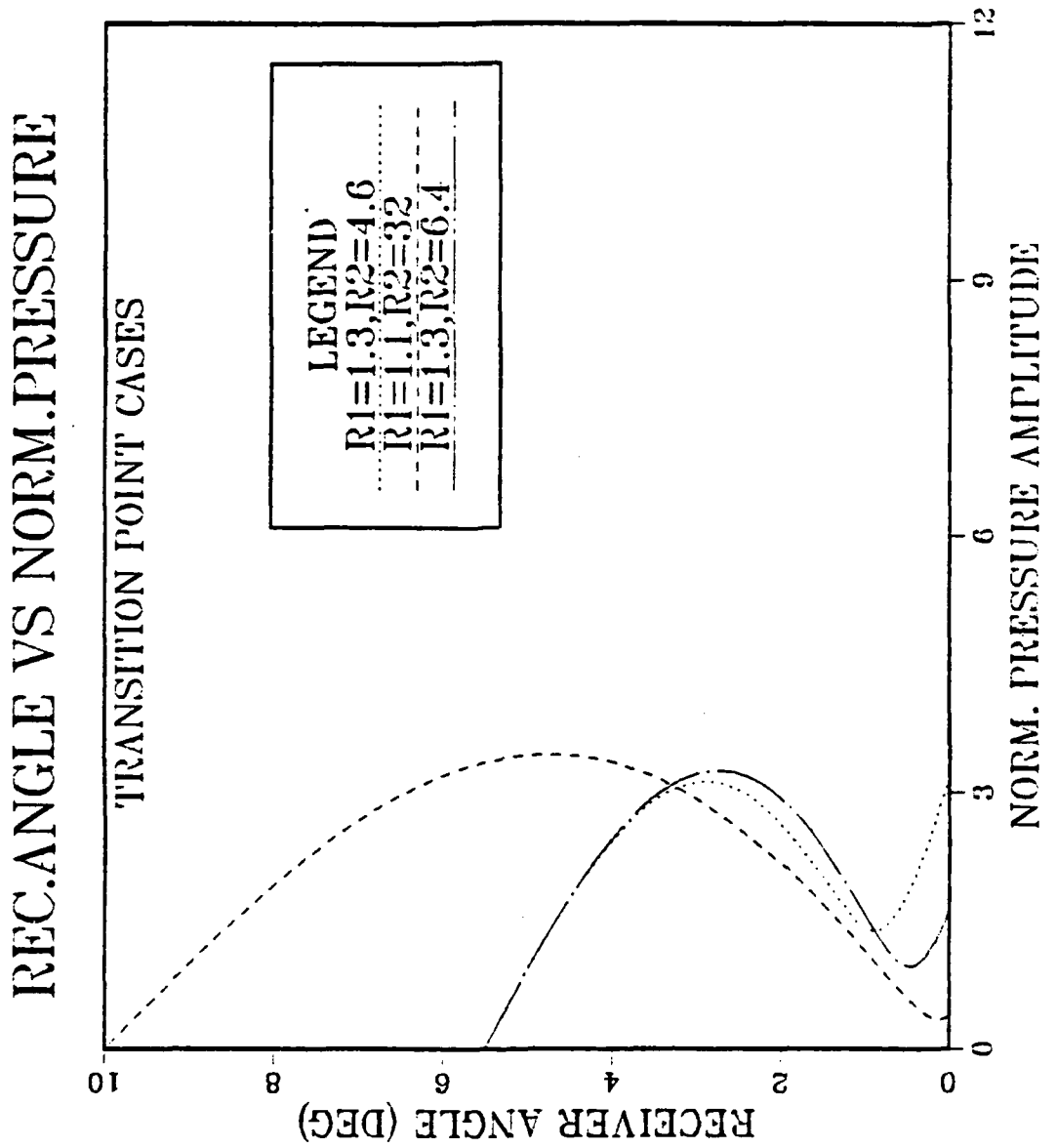

Figure 9. **Examples of Transition Points.**

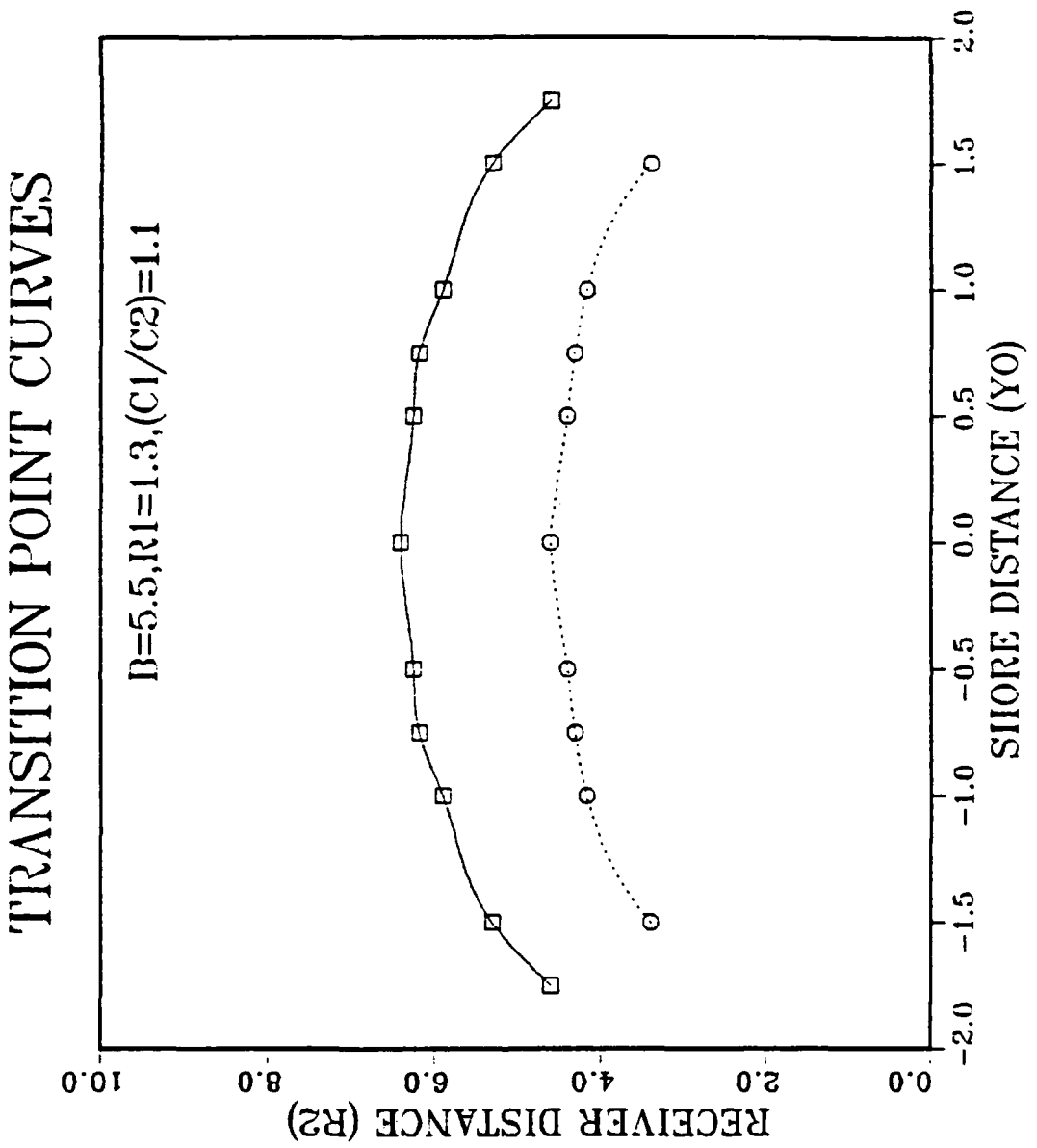

Figure 10. Transition Point Curves

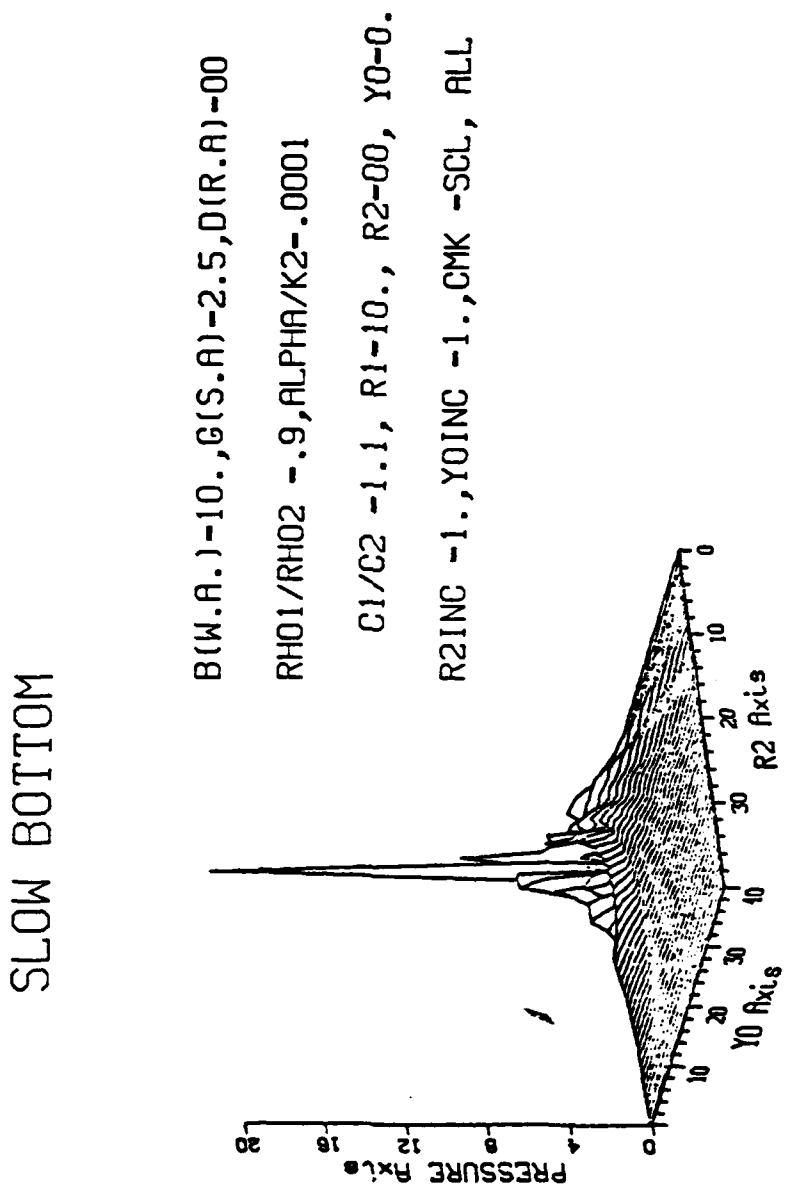

Figure 10A. **Pressure Distribution along the Bottom (G = 2.5)**

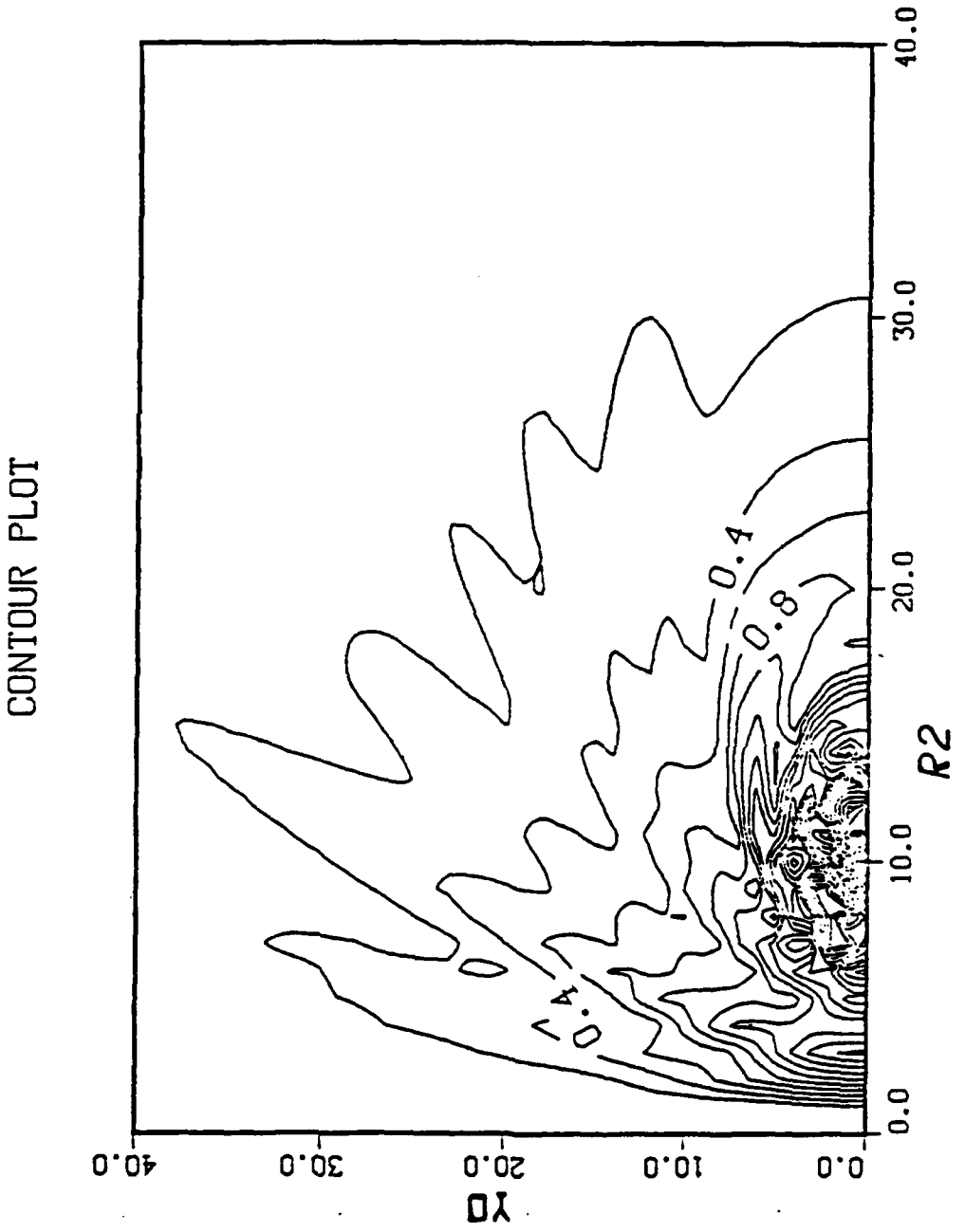

Figure 10B. Pressure Contour Plot Along the Bottom (G = 2.5)

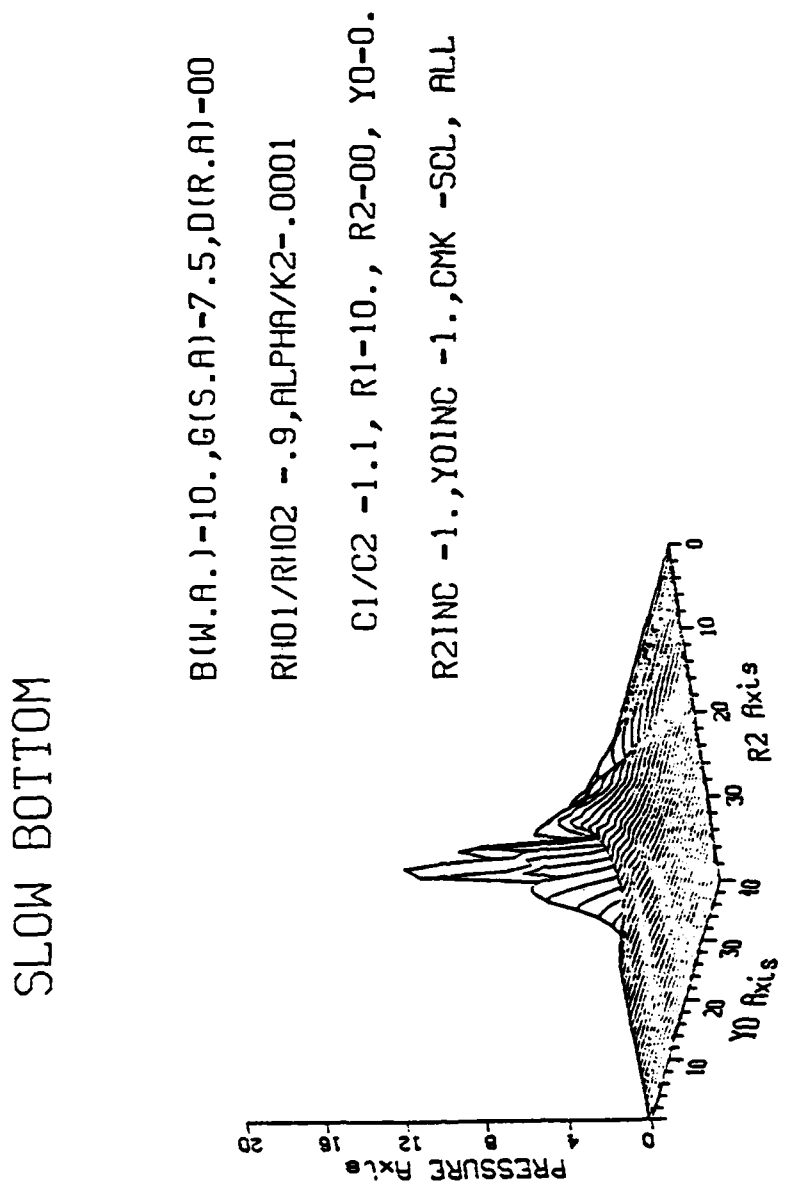

Figure 10C. **Pressure Distribution along the Bottom (G = 7.5)**

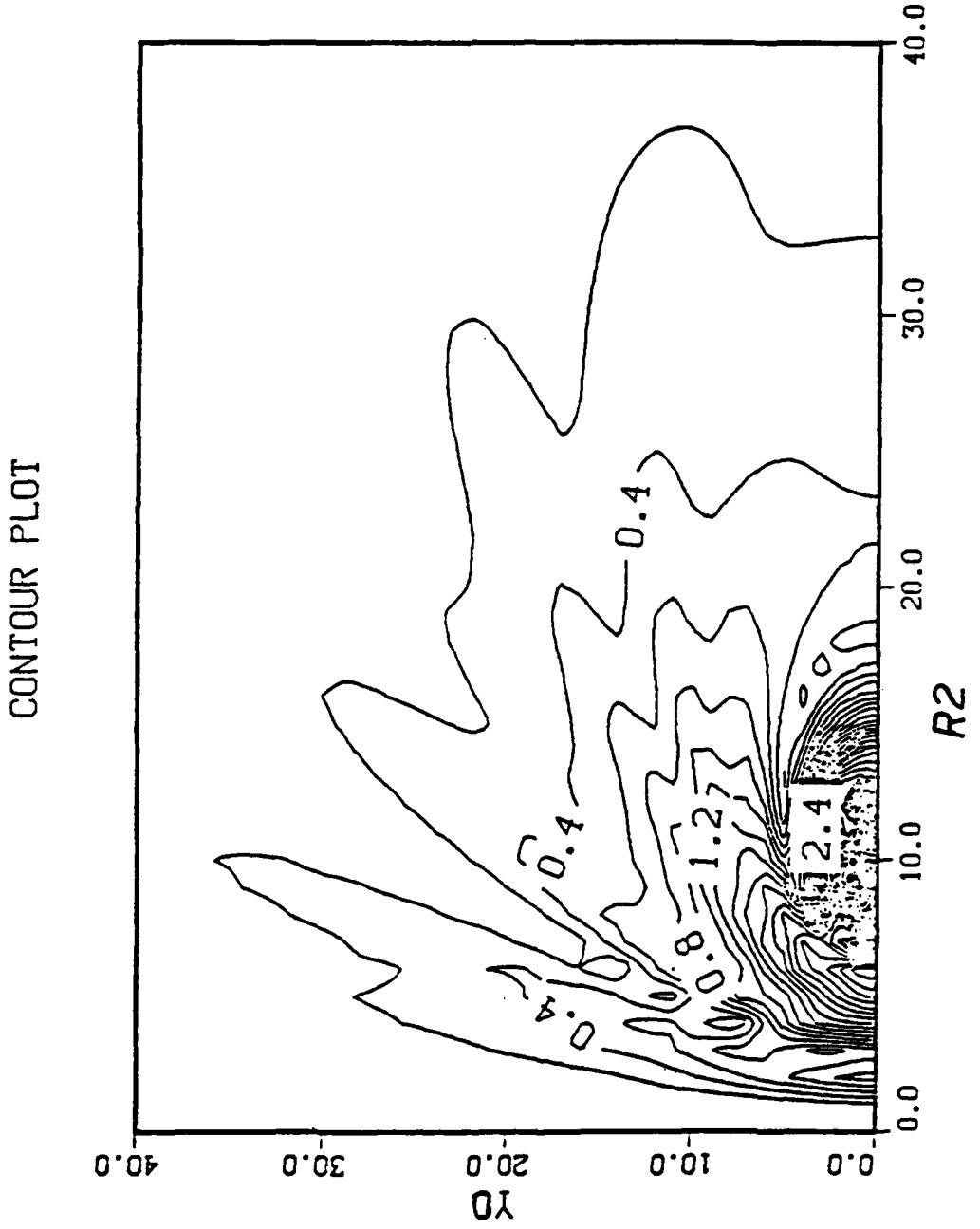

Figure 10D. Pressure Contour Plot Along the Bottom (G = 7.5)

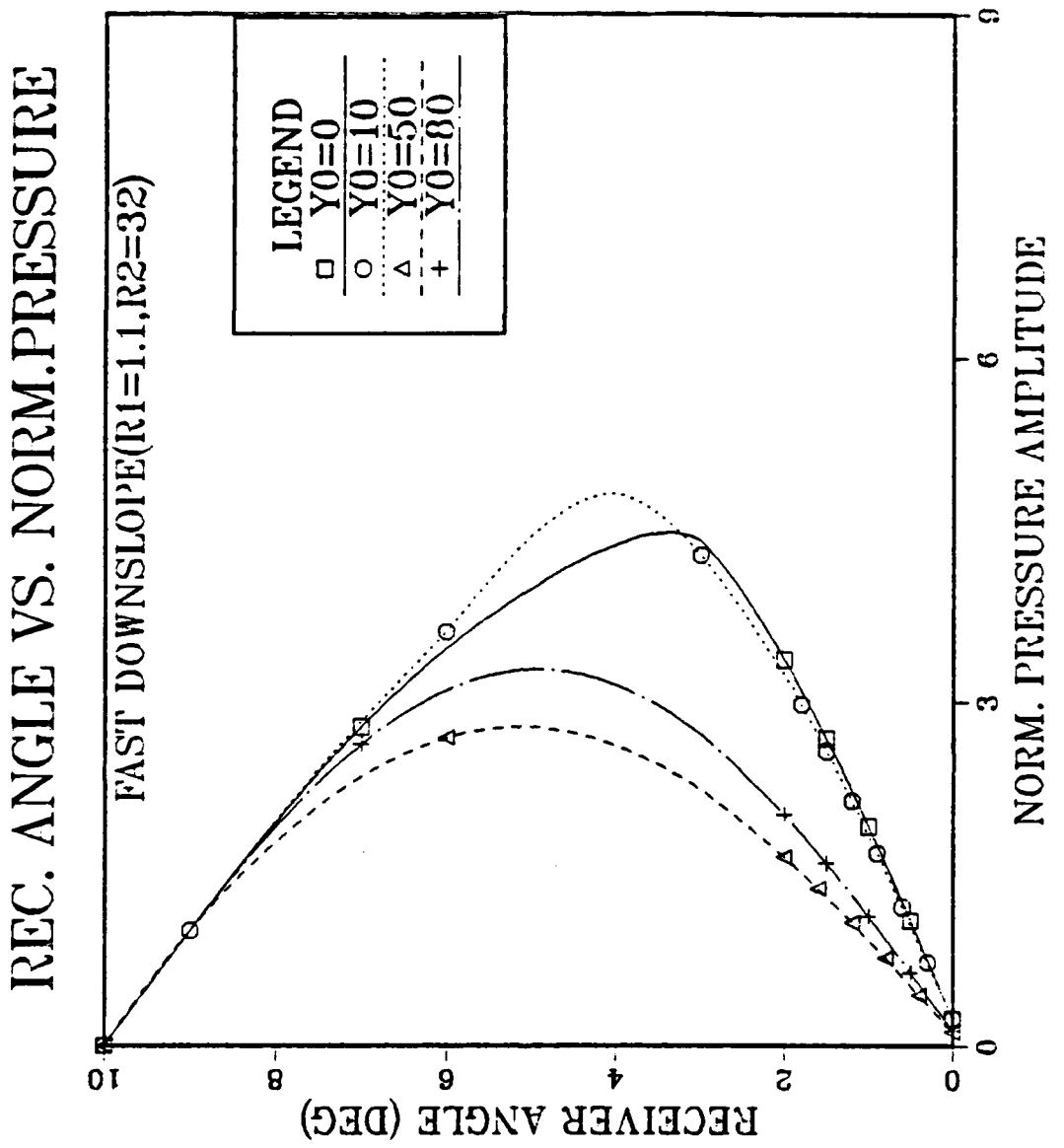

Figure 11. **Pressure Amplitude at R1=1.1 and R2=32 for Various Y0 over a Fast Bottom. (For clarity only every 5th computation shown)**

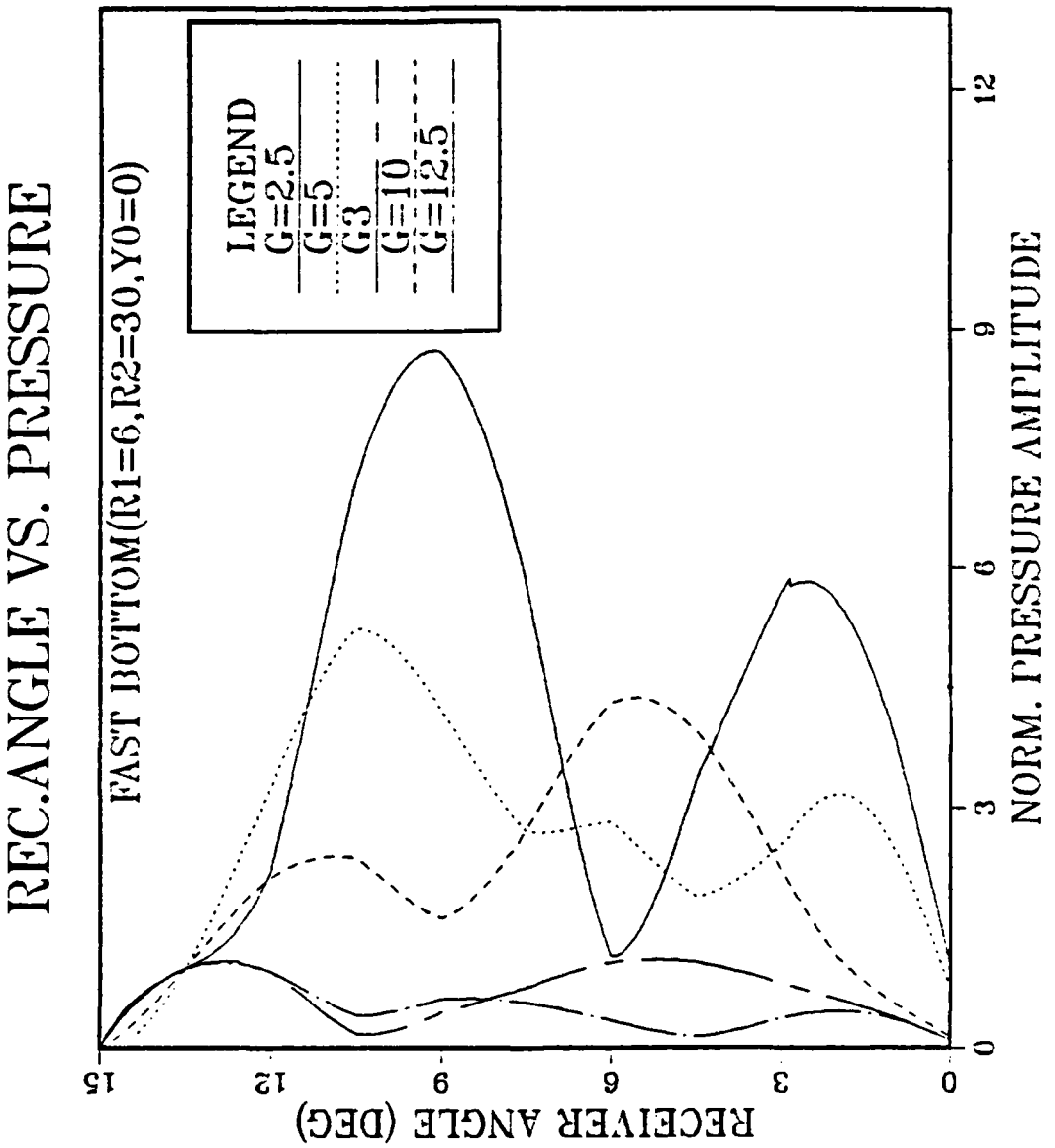

Figure 12. **Pressure Amplitude at R1=6,R2=30 and Y0=0 for Various G over a Fast Bottom.**

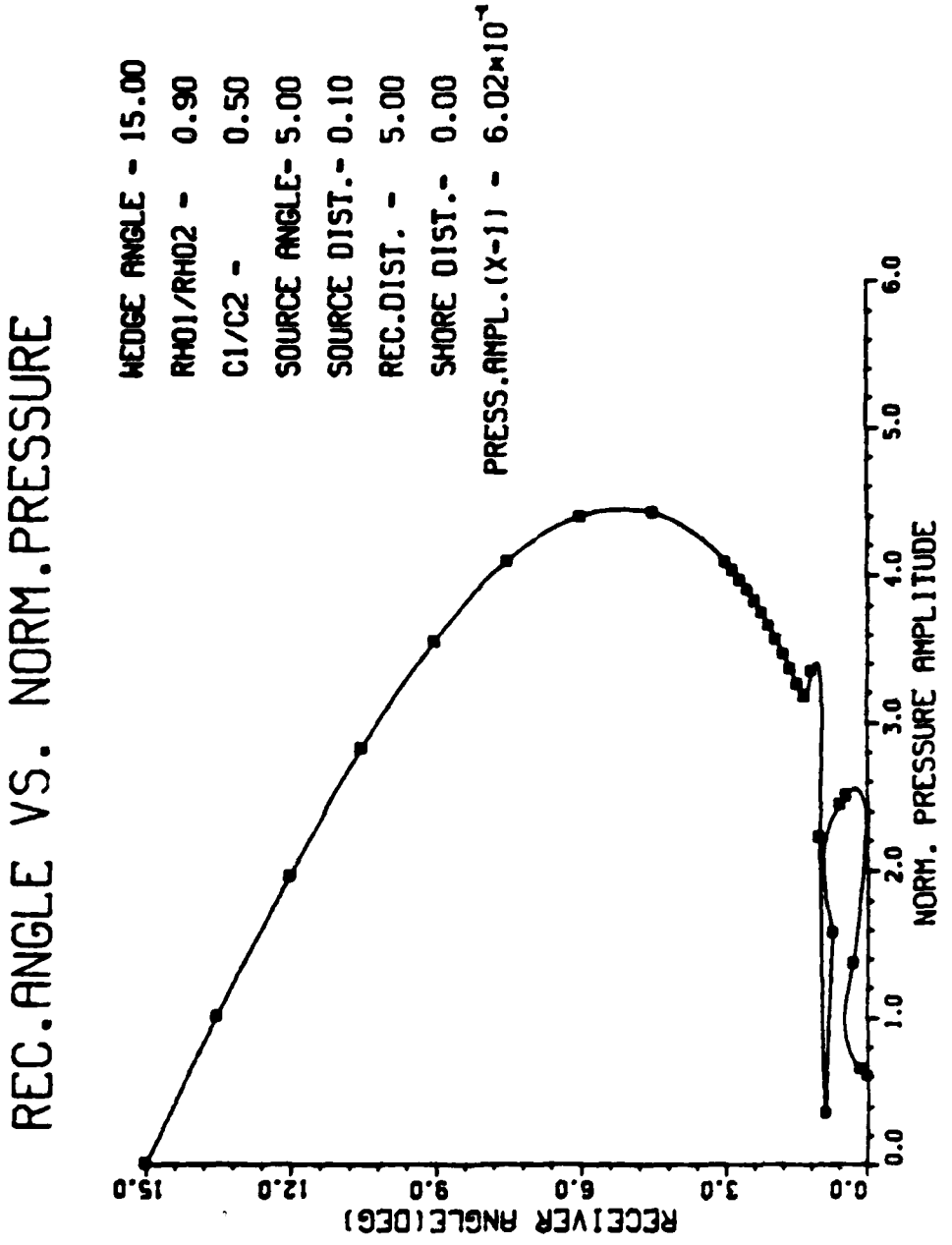

Figure 13. Pressure Amplitude at R1=0.1,R2=5,Y0=0 Over a Fast Bottom

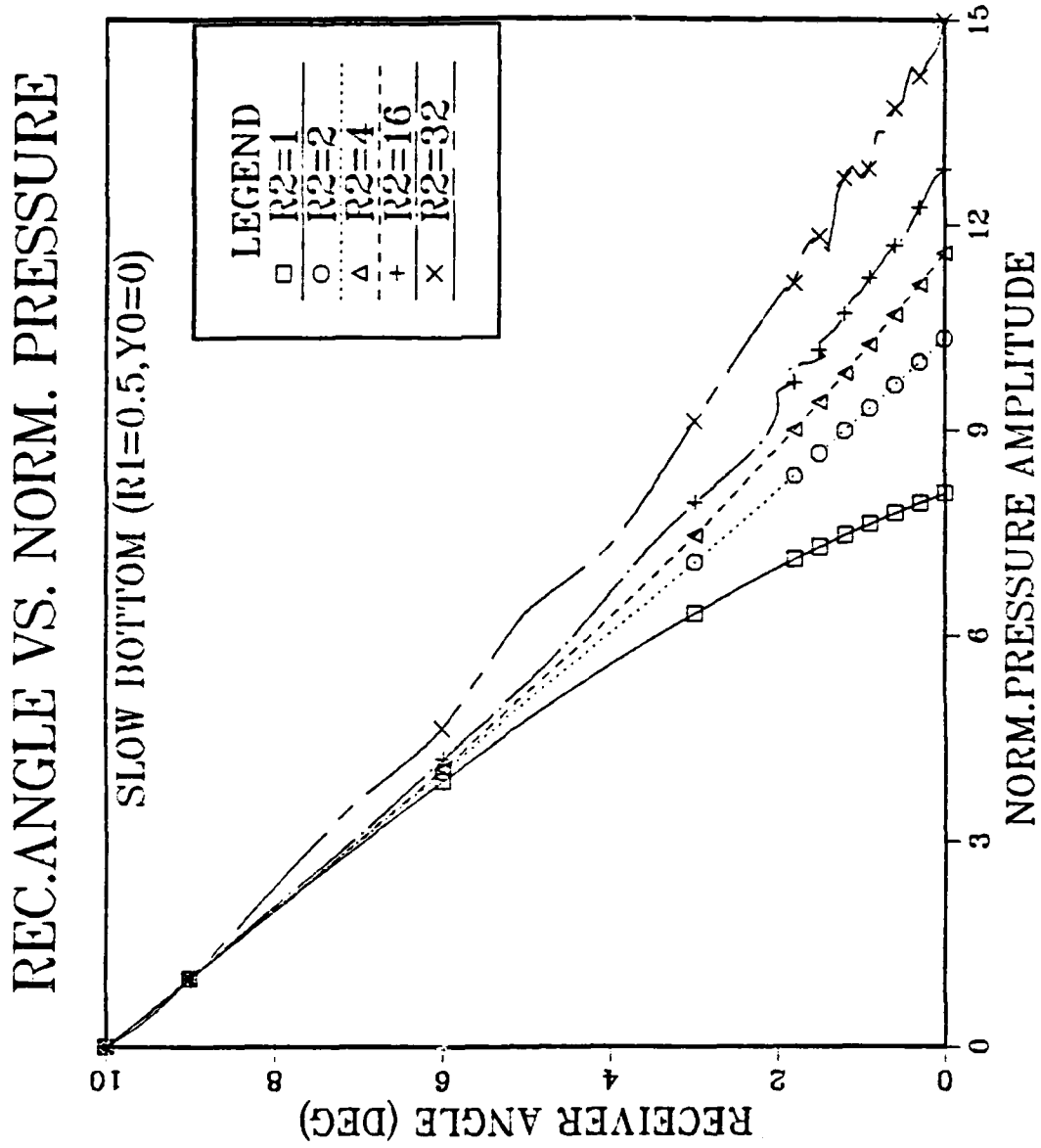

Figure 14. **Pressure Amplitude at R1=0.5, Y0=0 for Various R2 over a Slow Bottom. (For clarity only every 5th computation shown)**

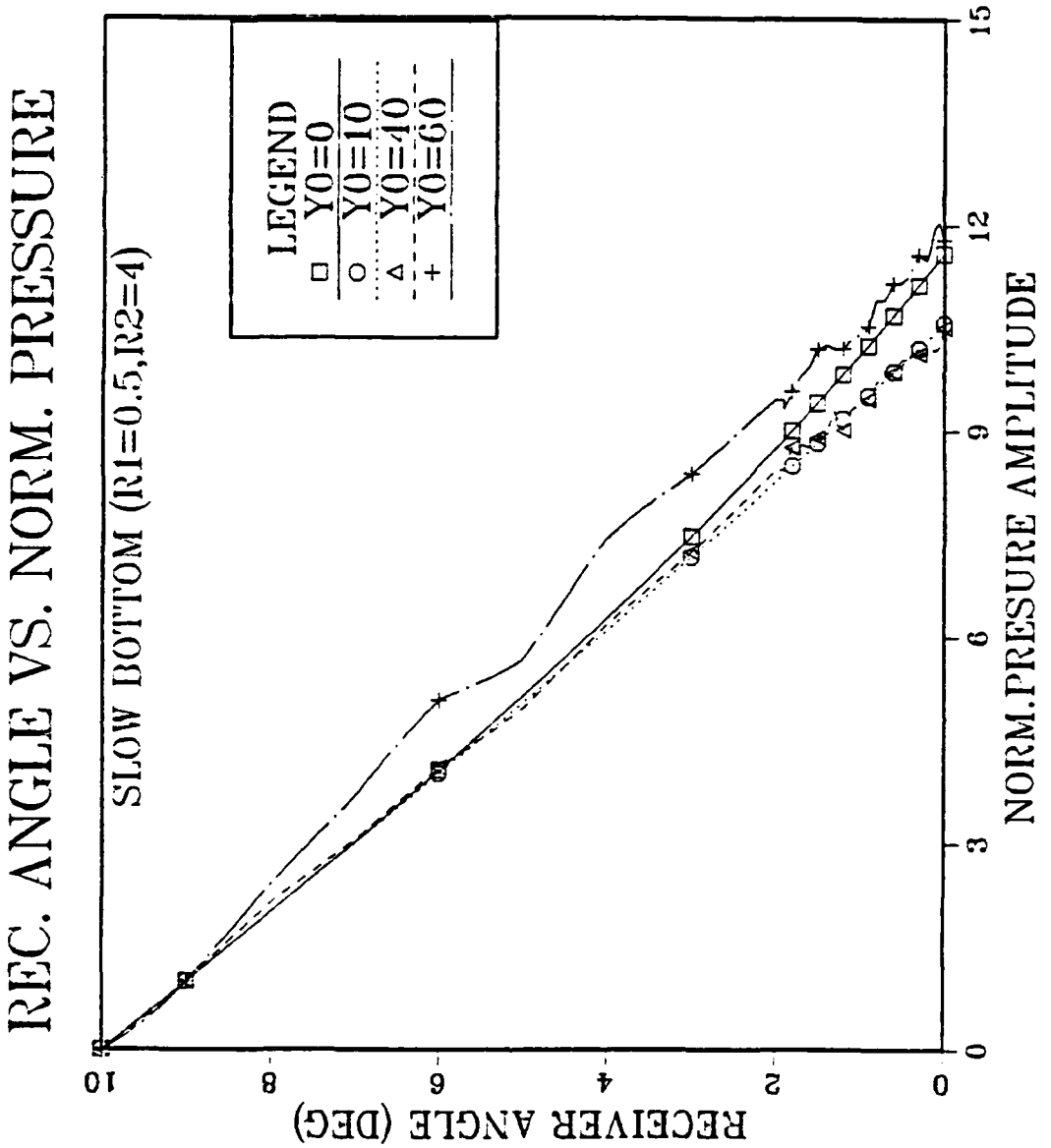

Figure 15. **Pressure Amplitude at R1=0.5, R2=4 for Various Y0 Over a Slow Bottom. (For clarity only every 5th computation shown)**

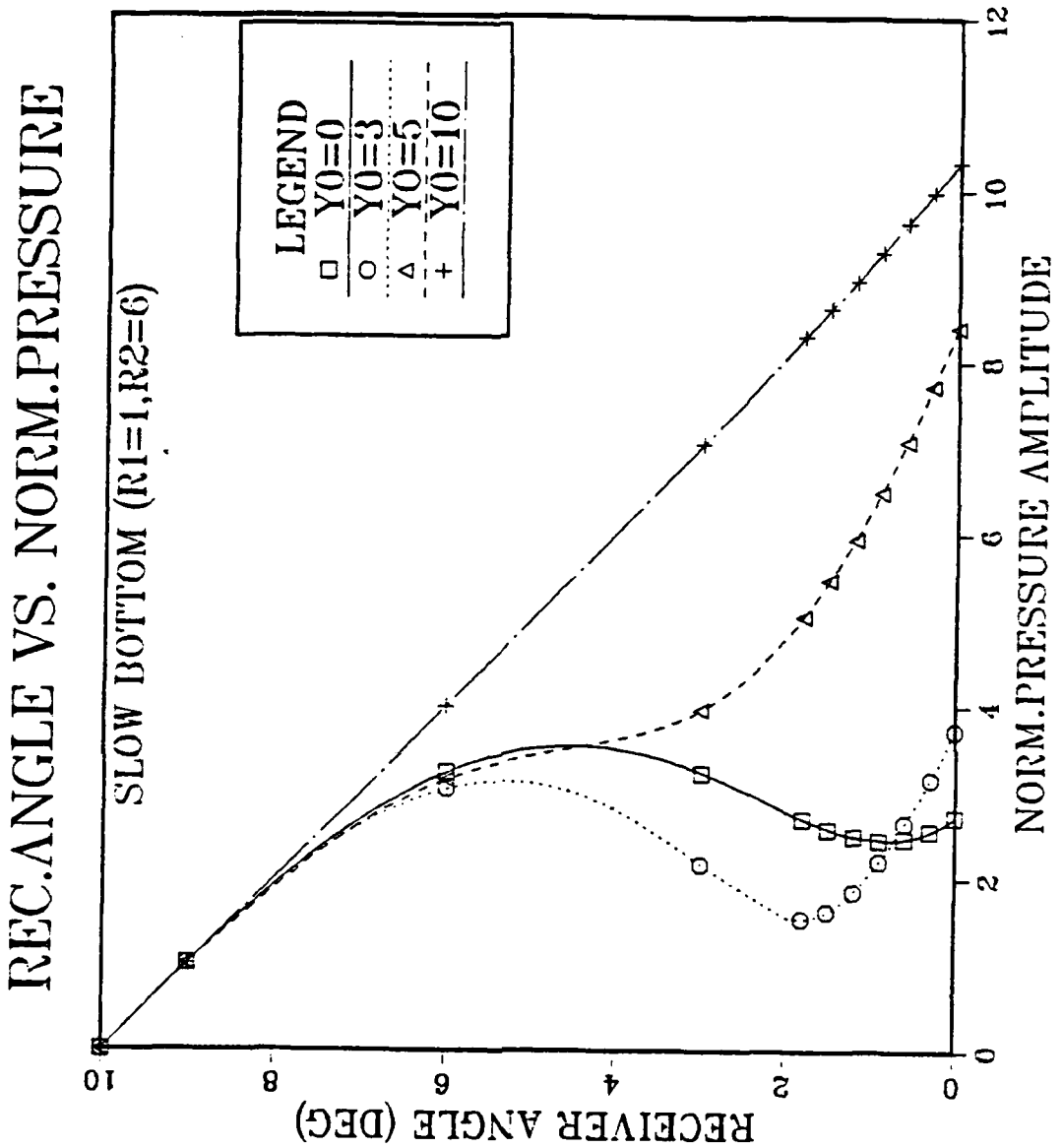

Figure 16. **Pressure Amplitude at R1=1, R2=6 for Various Y0 over a Slow Bottom. (For clarity only every 5th computation shown)**

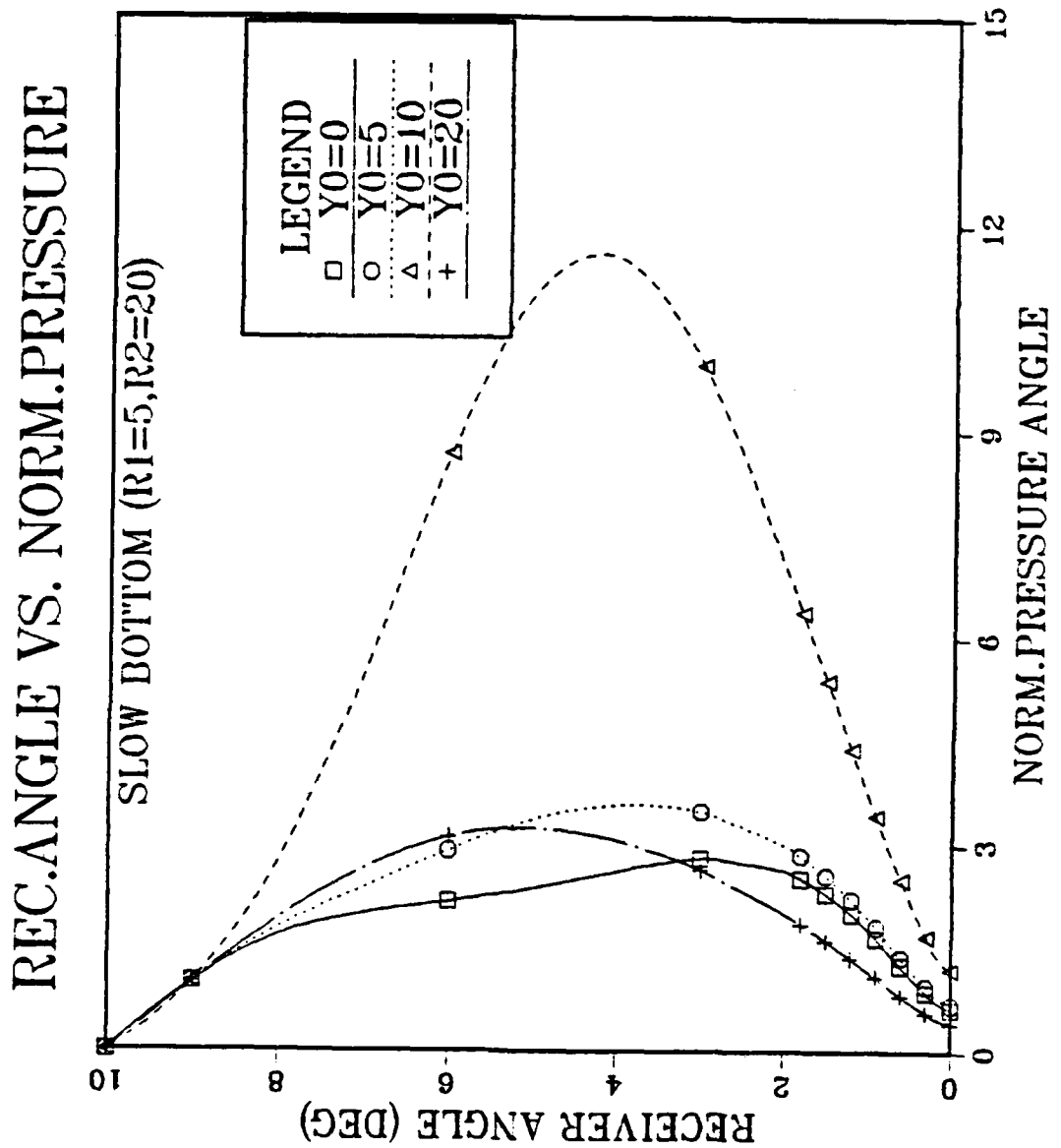

Figure 17. **Pressure Amplitude at R1=5, R2=20 for Various Y0 Over a Slow Bottom. (For clarity only every 5th computation shown)**

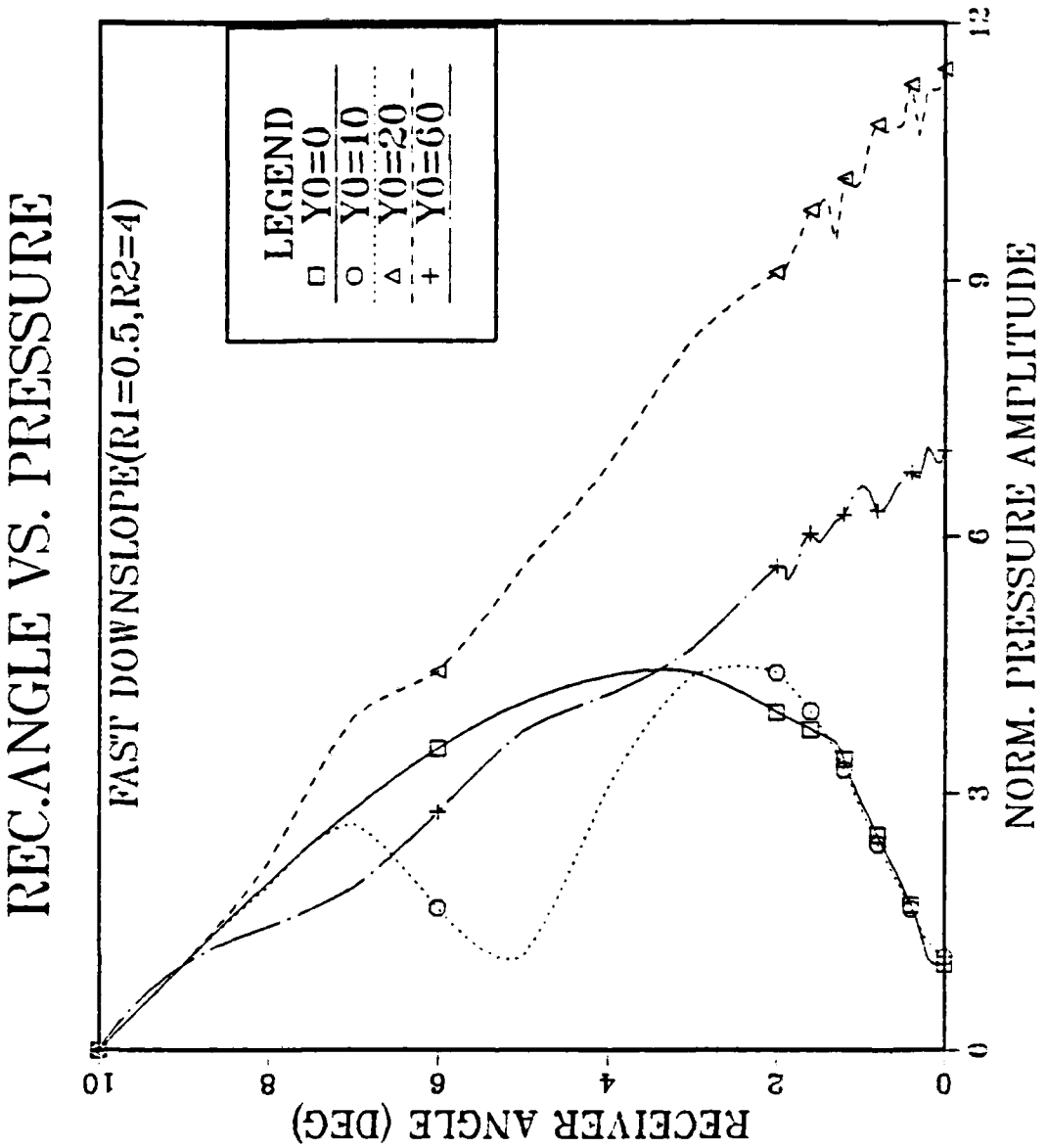

Figure 18. **Pressure Amplitude at R1=0.5, R2=4 for Various Y0 Over a Fast Bottom. (For clarity only every 5th computation shown)**

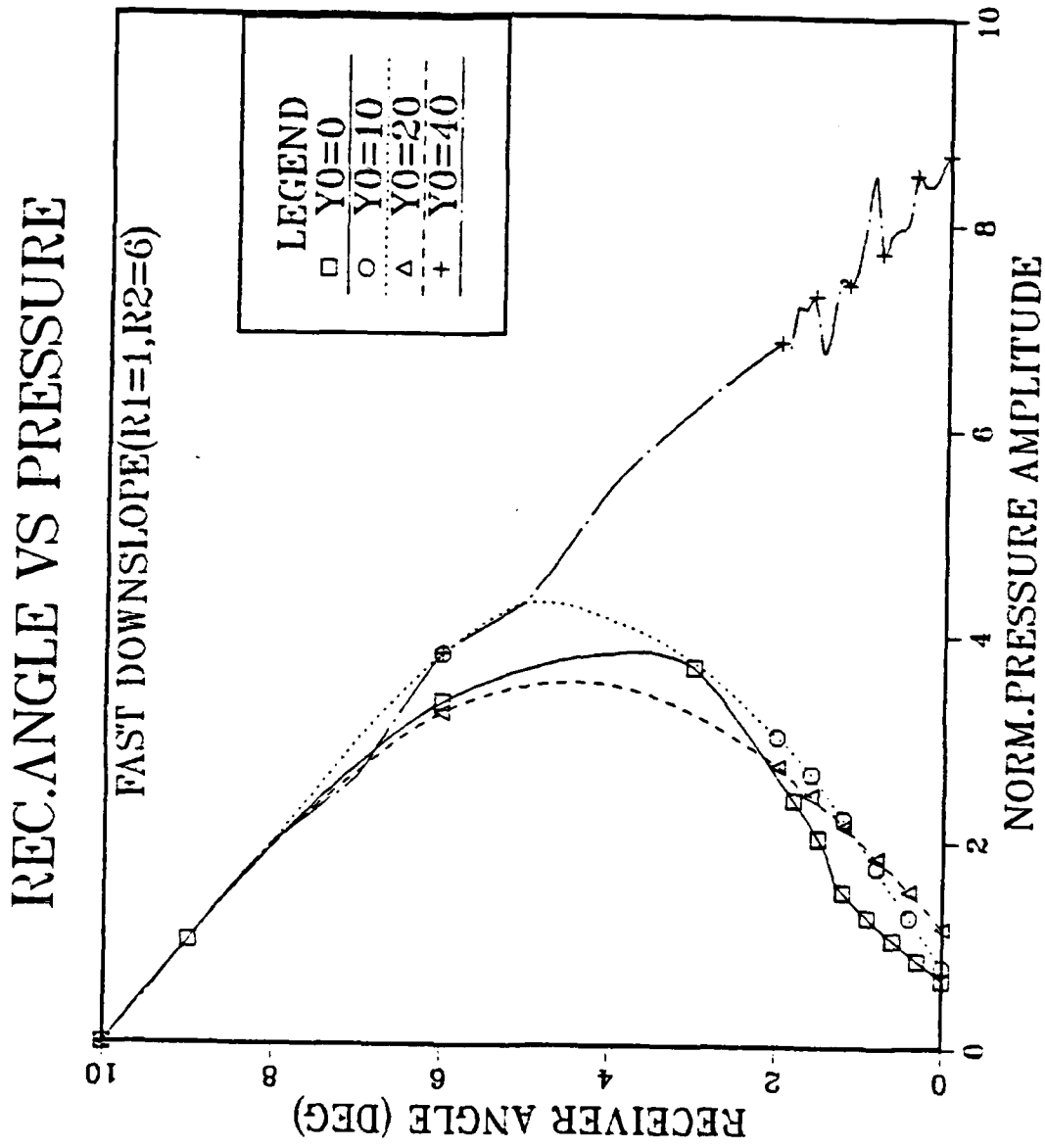

Figure 19. **Pressure Amplitude at R1=1, R2=6 For Various Y0 Over a Fast Bottom. (For clarity only every 5th computation shown)**

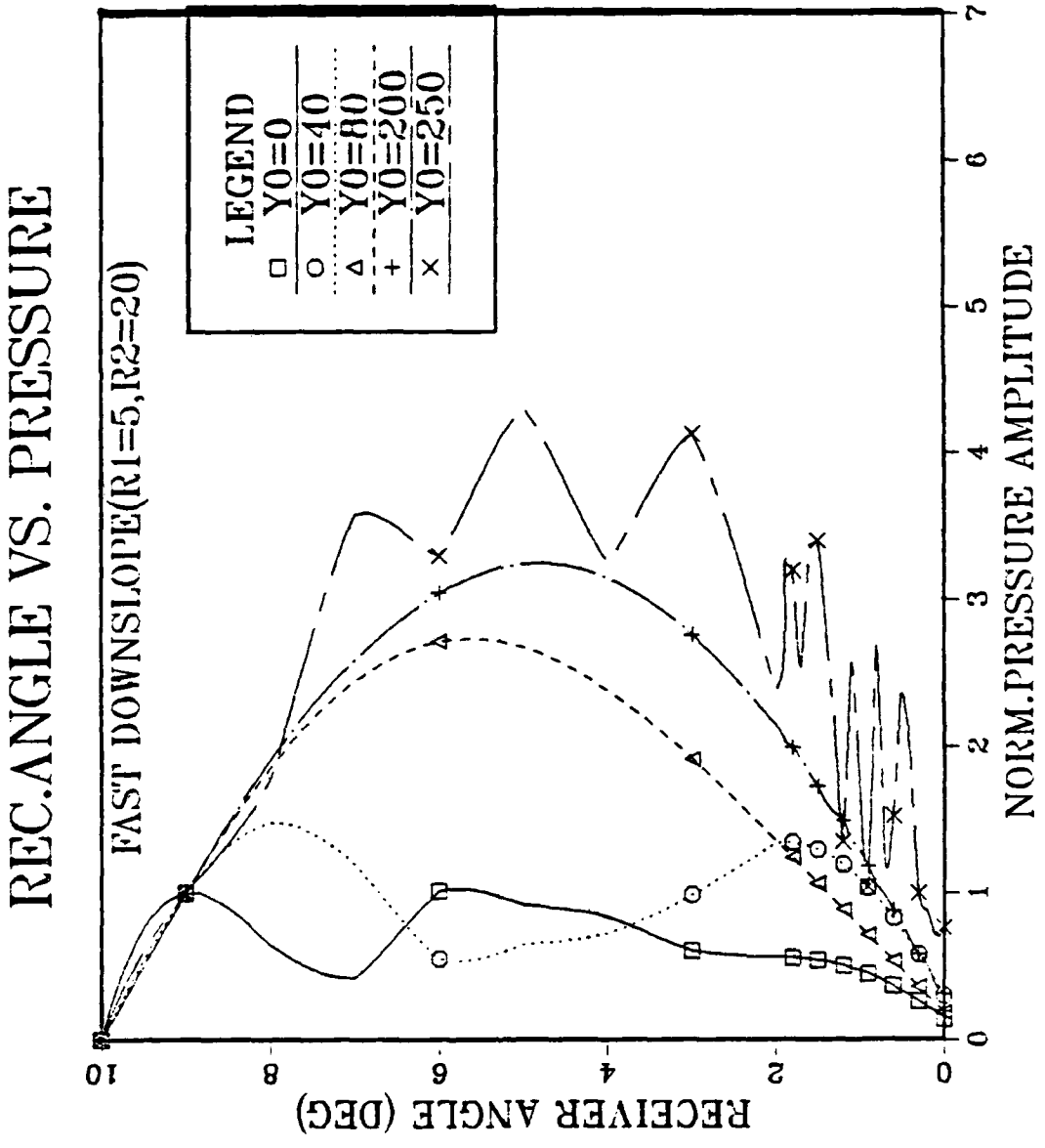

Figure 20. **Pressure Amplitude at R1=5, R2=20 for Various Y0 Over a Fast Bottom. (For clarity only every 5th computation shown)**

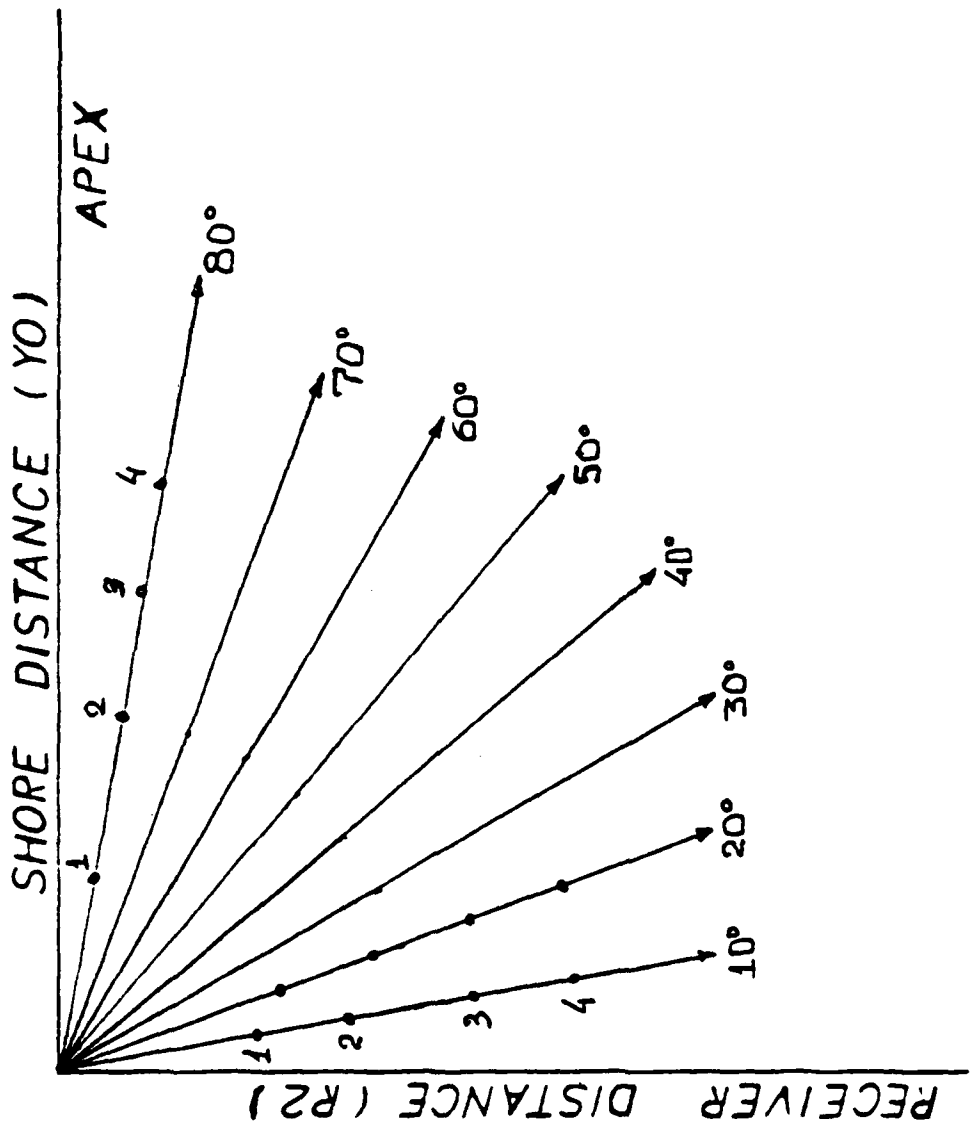

Figure 21. Searching Pattern of the Angular Output Data

Figure 22. Pressure Distribution over a Slow Bottom (R1 = 10)

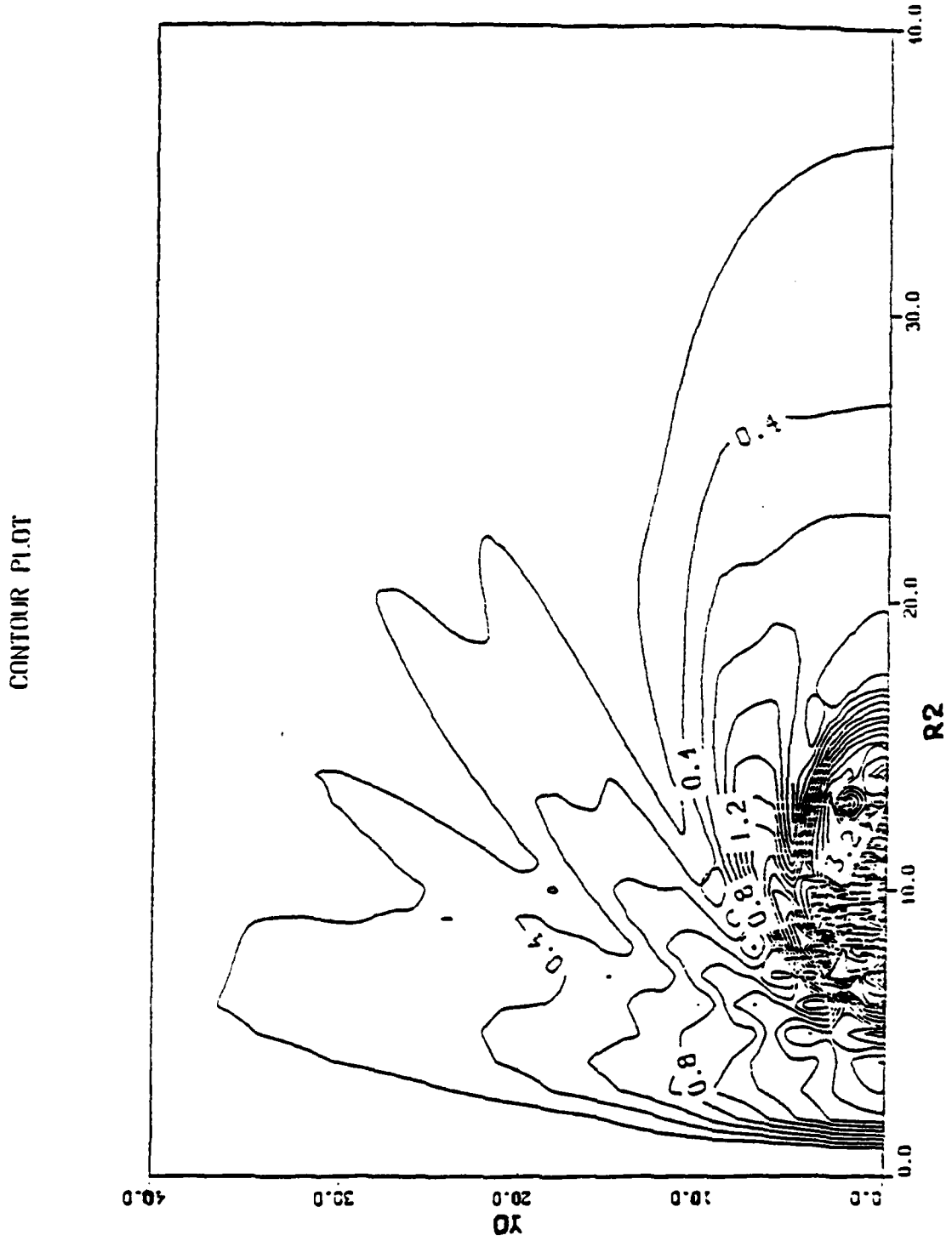

Figure 23. Pressure Contour Plot over a Slow Bottom (R1 = 10)

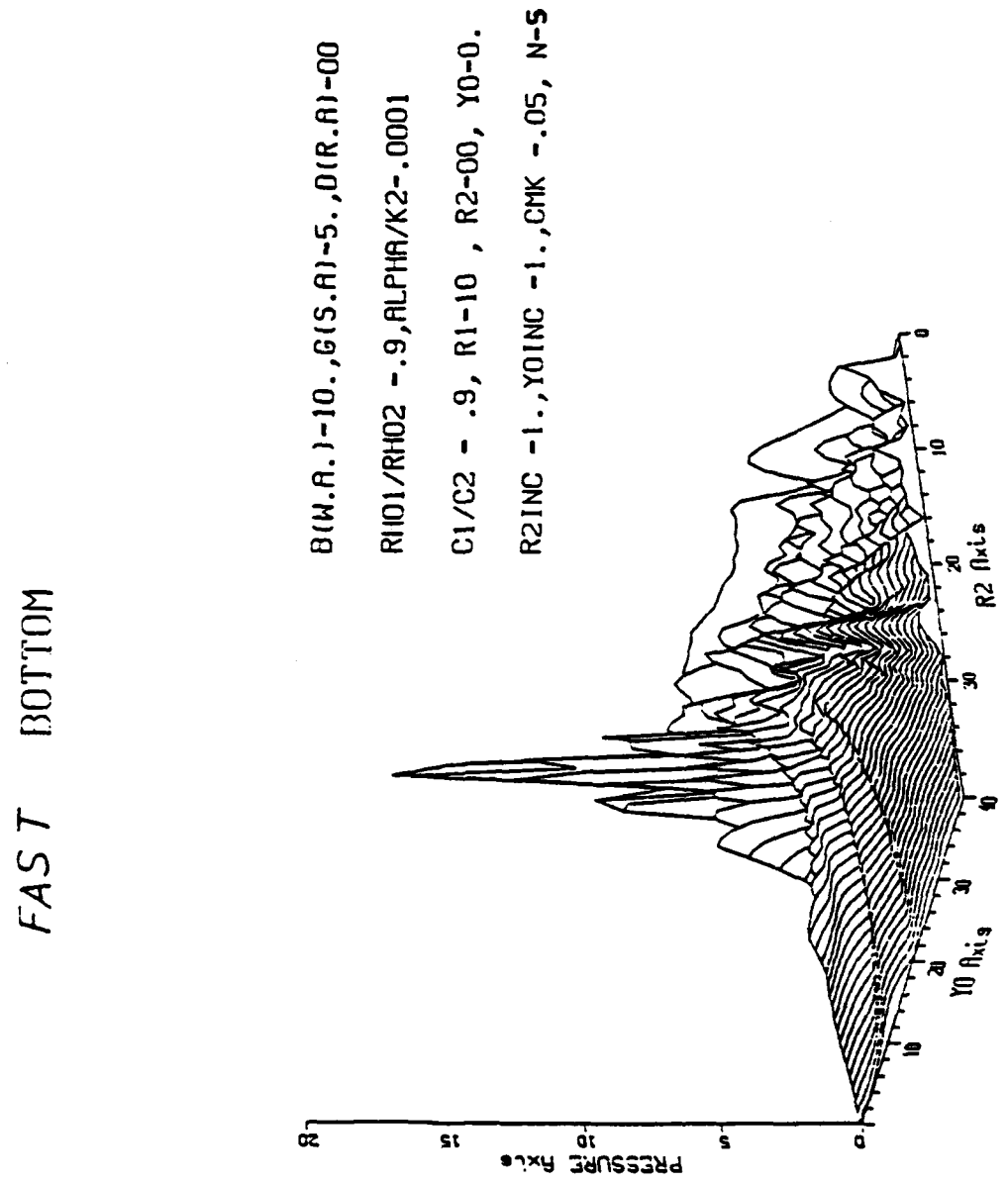

Figure 24. **Pressure Distribution over a Fast Bottom (R1 = 10)**

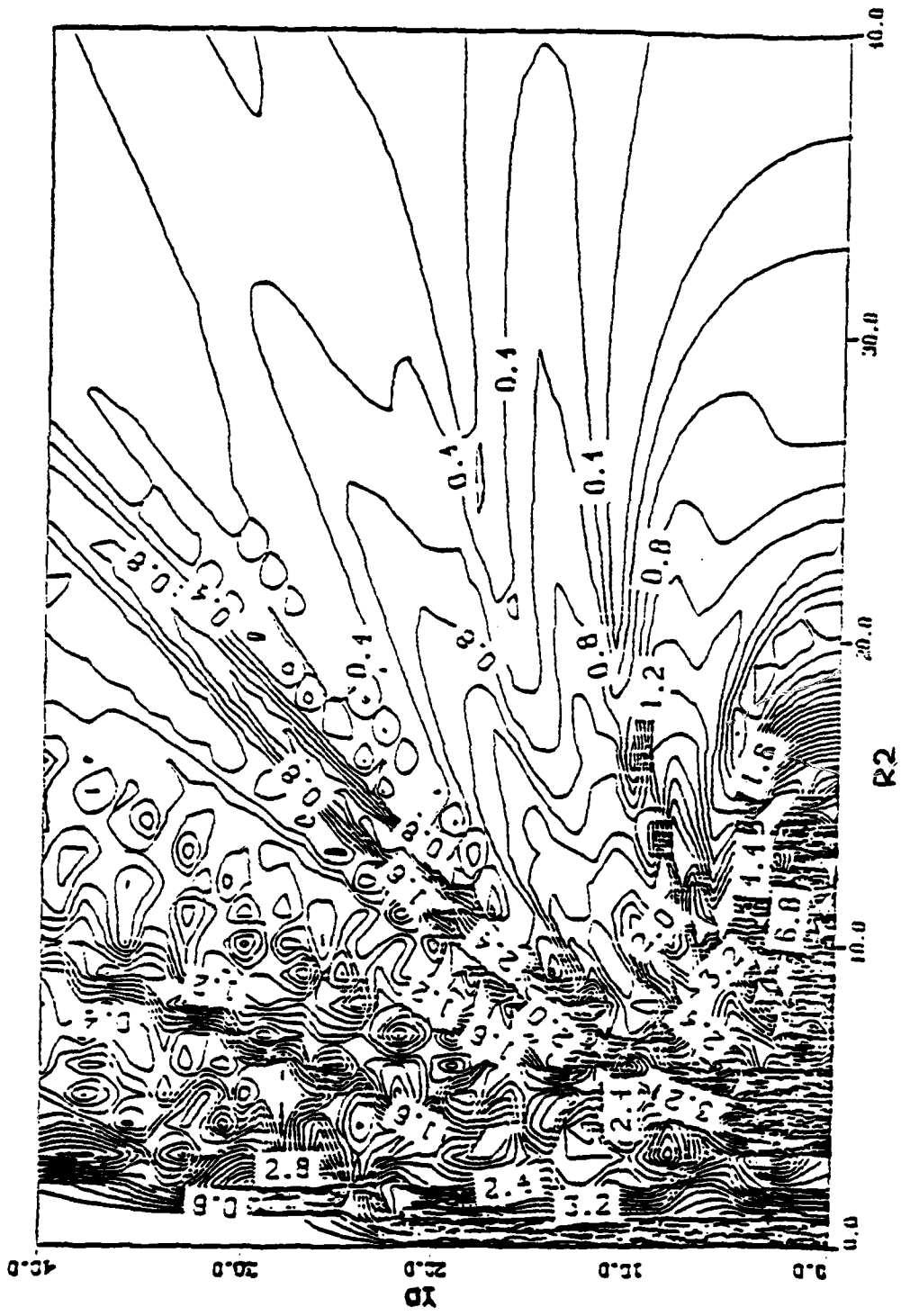

Figure 25. Pressure Contour Plot over a Fast Bottom (R1 = 10)

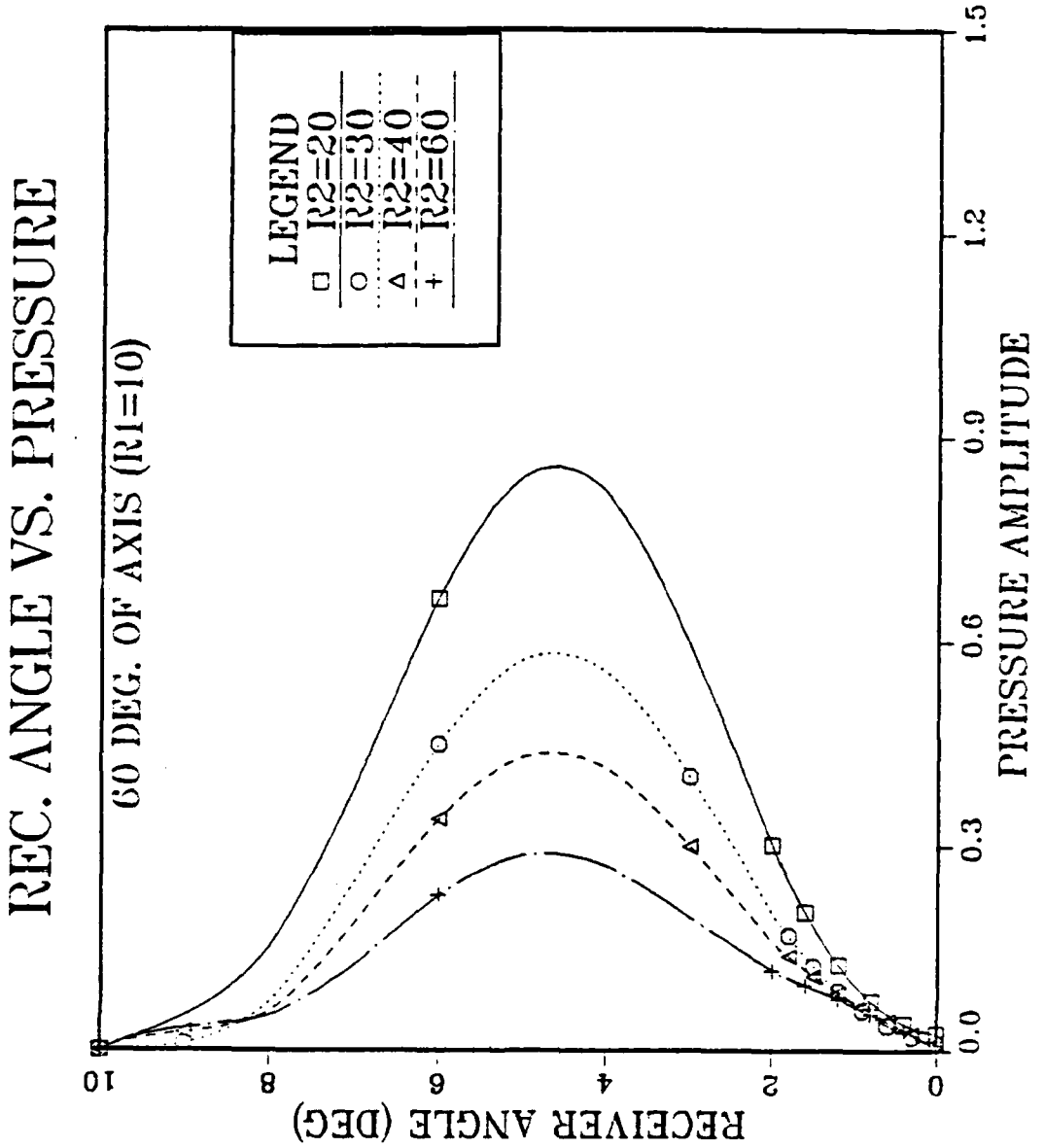

Figure 26. **Pressure Amplitude at 60° off Axis (R1=10) for Various R2 over a Slow Bottom. (For clarity only every 5th computation shown)**

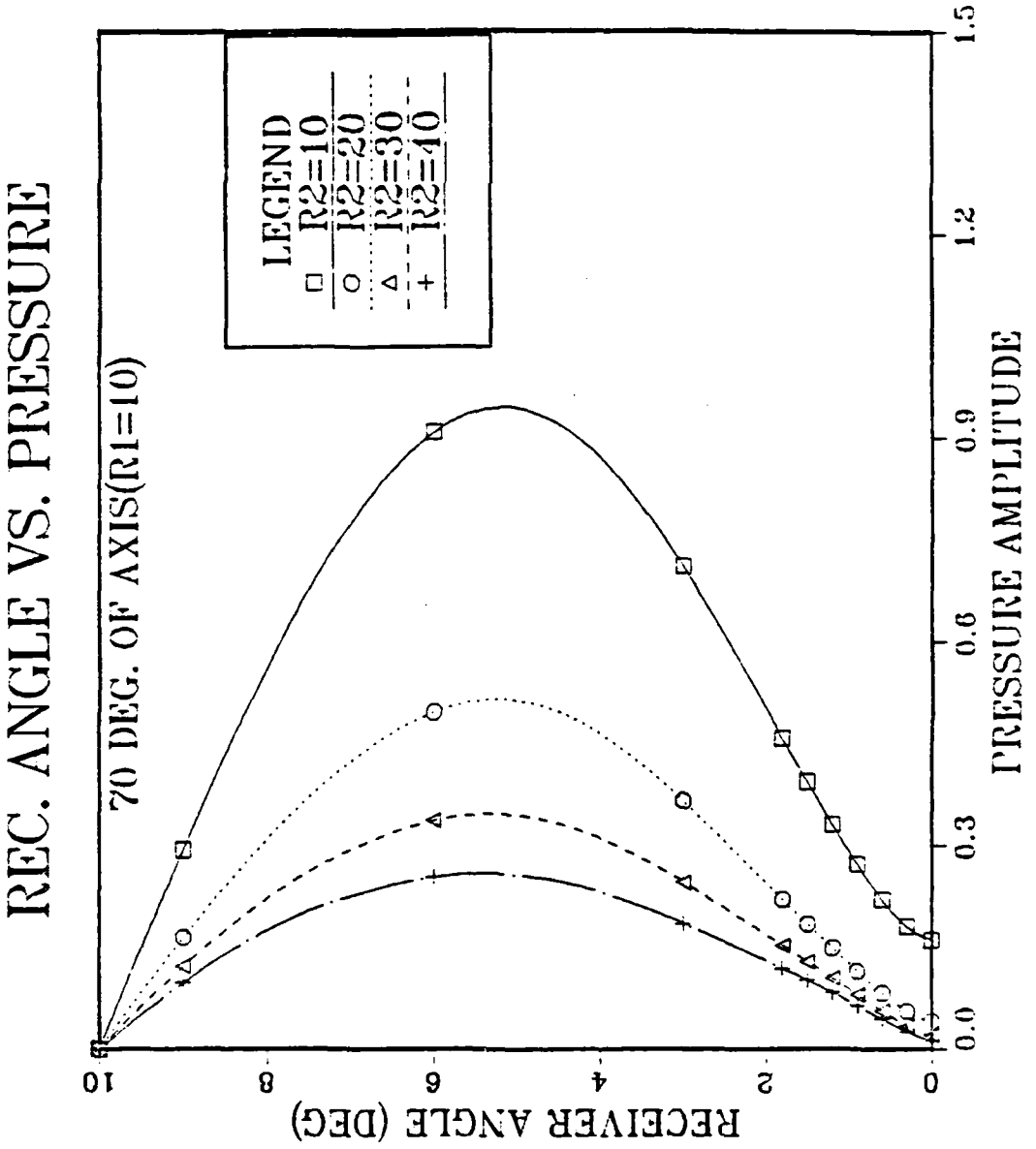

Figure 27. **Pressure Amplitude at 70° off Axis for Various R2 (R1=10) over a Slow Bottom. (For clarity only every 5th computation shown)**

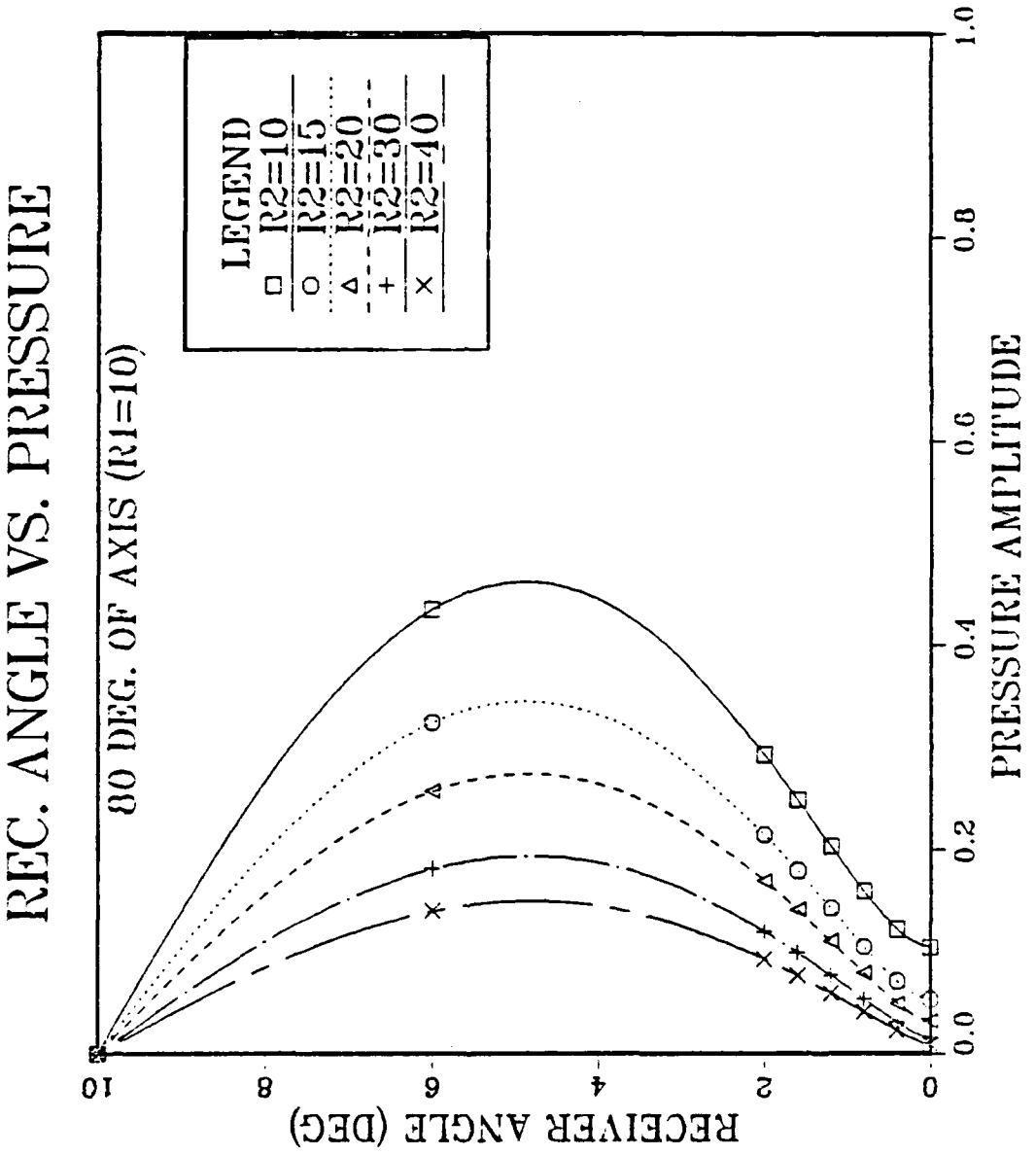

Figure 28. **Pressure Amplitude at 80° off Axis for Various R2 (R1=10) over a Slow Bottom. (For clarity only every 5th computation shown)**

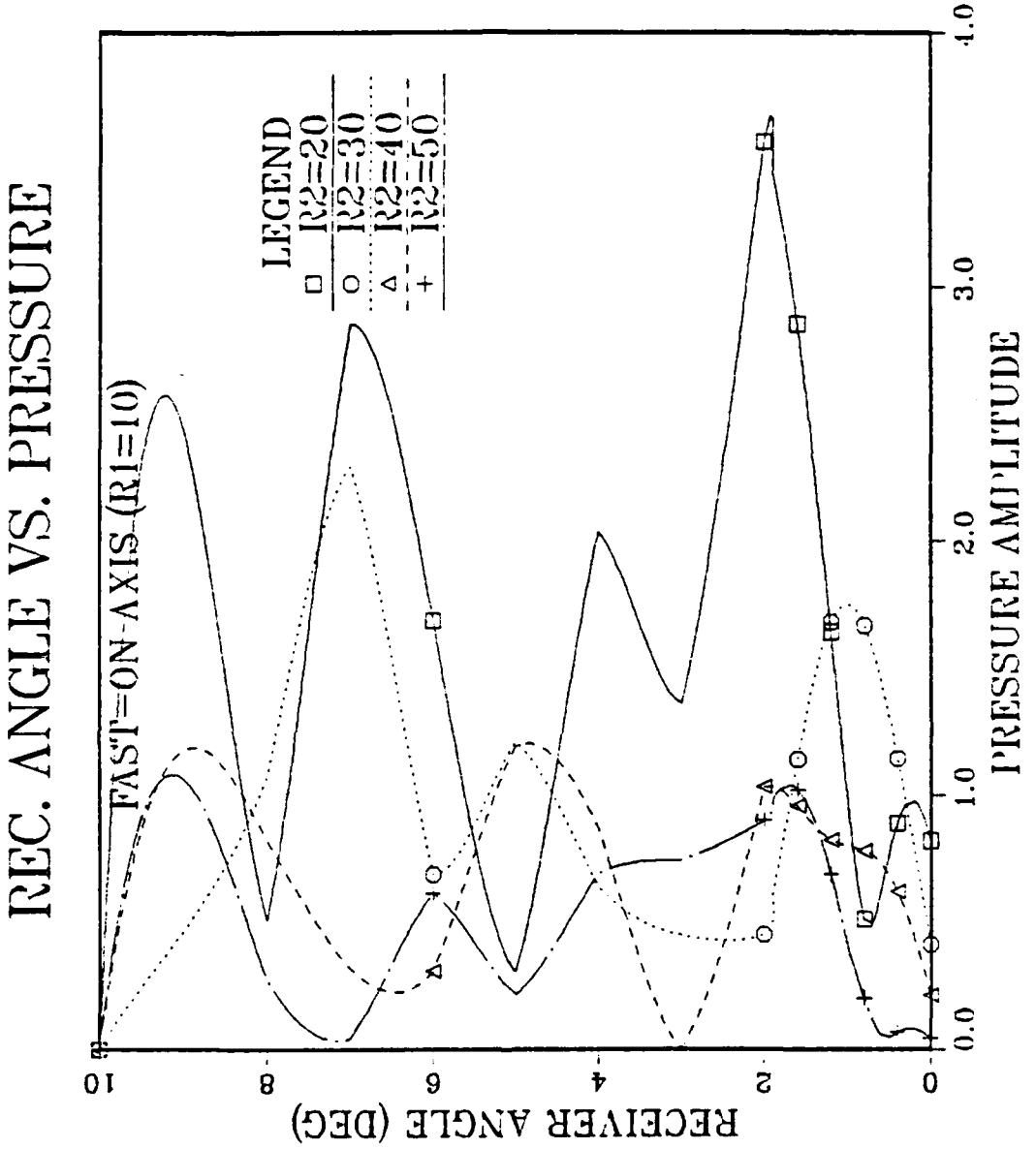

Figure 29. **Pressure Amplidute on Axis (R1=10) for Various R2 Over a Fast Bottom. (For clarity only every 5th computation shown)**

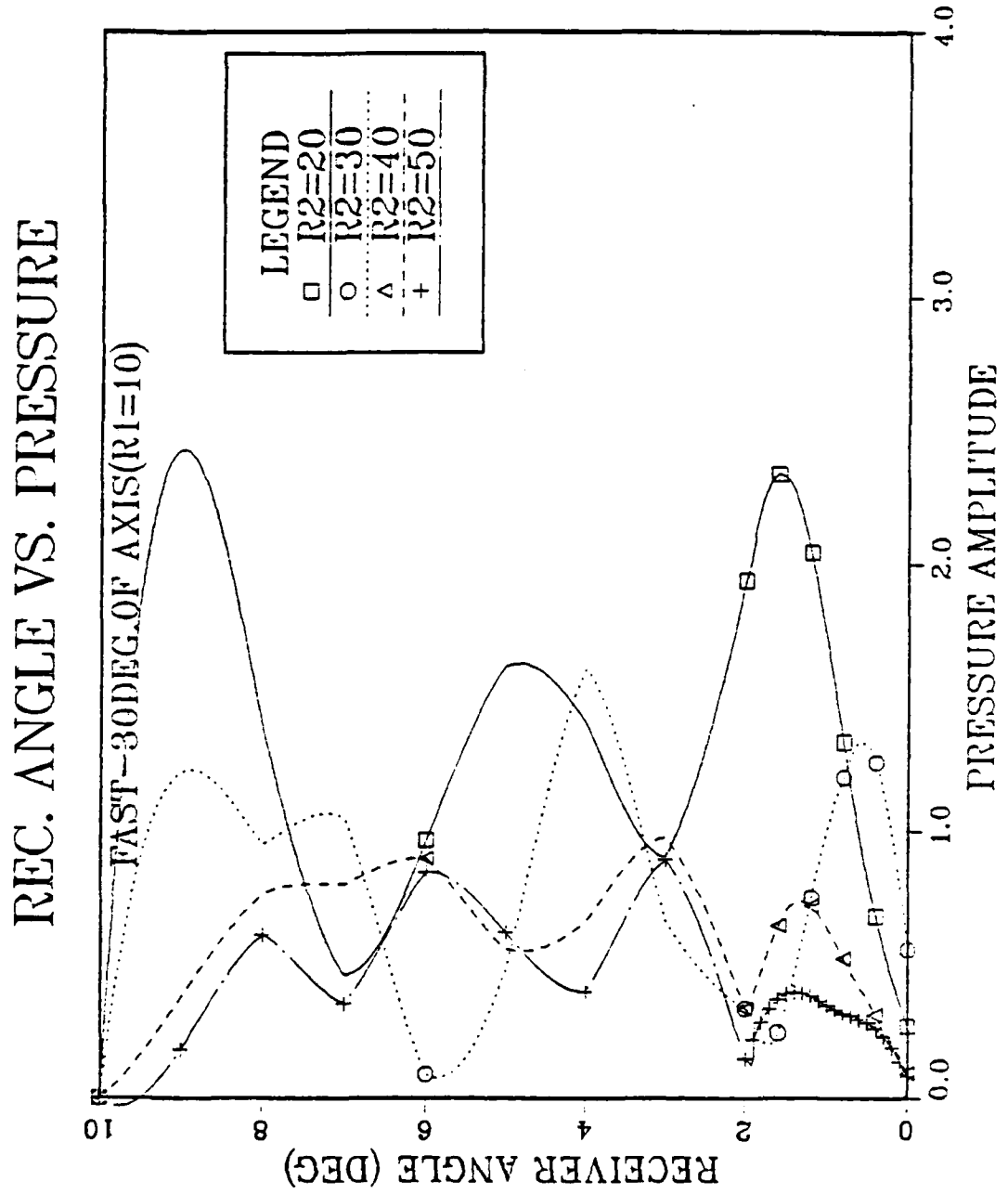

Figure 30. **Pressure Amplitude 30° of Axis for Various R2 (R1=10) over a Fast Bottom. (For clarity only every 5th computation shown)**

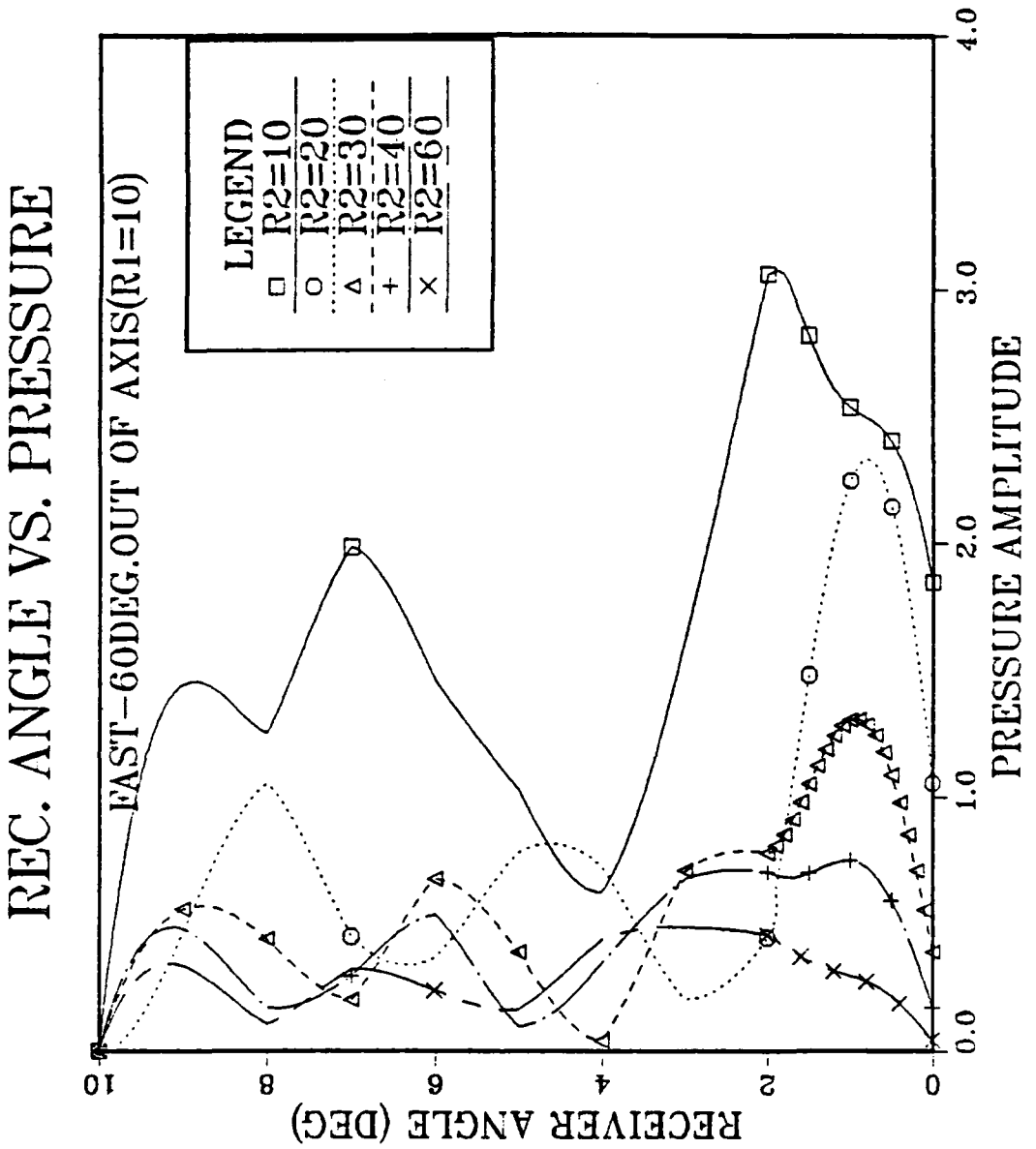

Figure 31. **Pressure Amplitude at 60° of Axis for Various R2 (R1=10) Over a Fast Bottom. (For clarity only every 5th computation shown)**

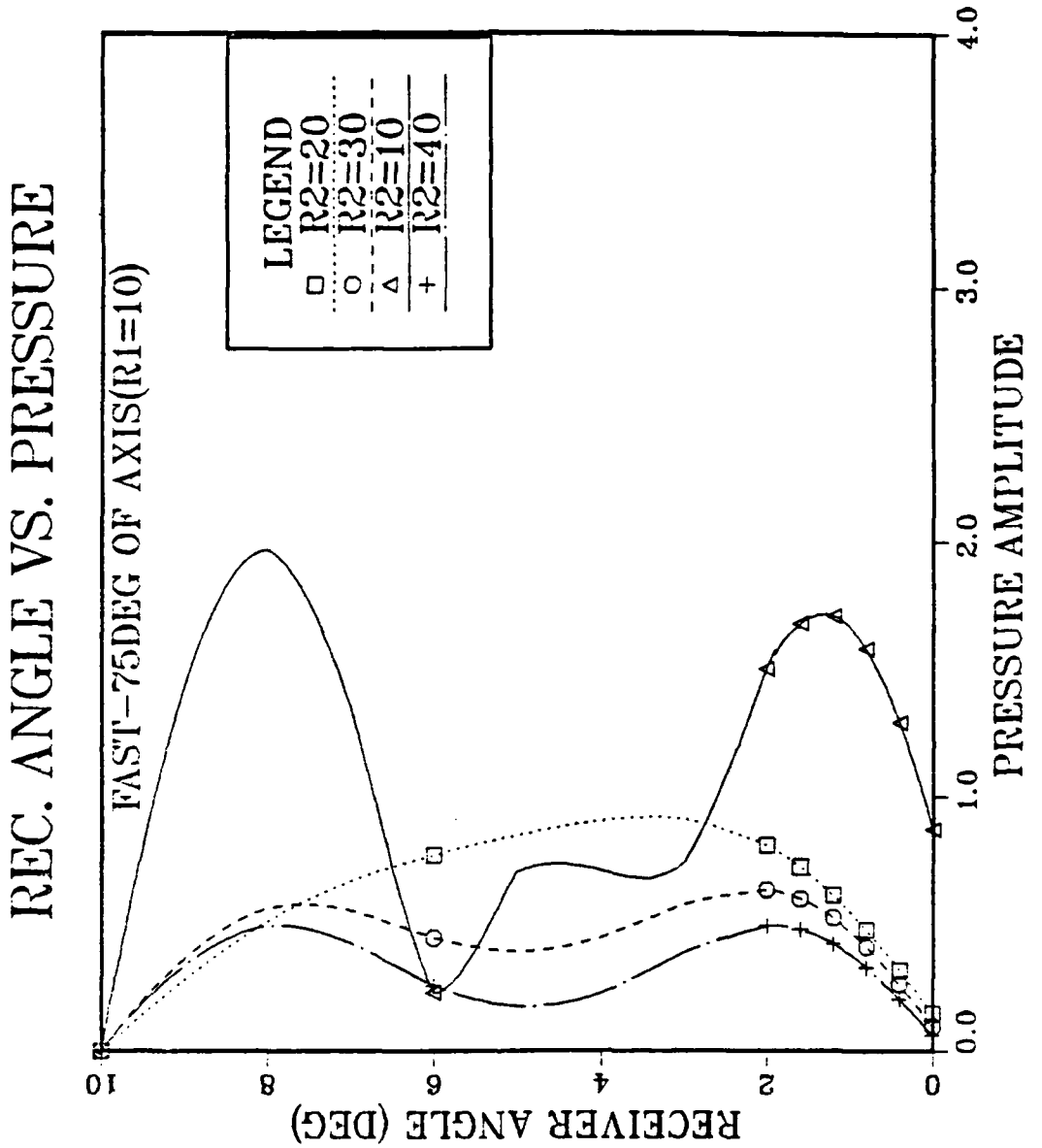

Figure 32. **Pressure Amplitude at 75° of Axis for Various R2 (R1=10) Over a Fast Bottom. (For clarity only every 5th computation shown)**

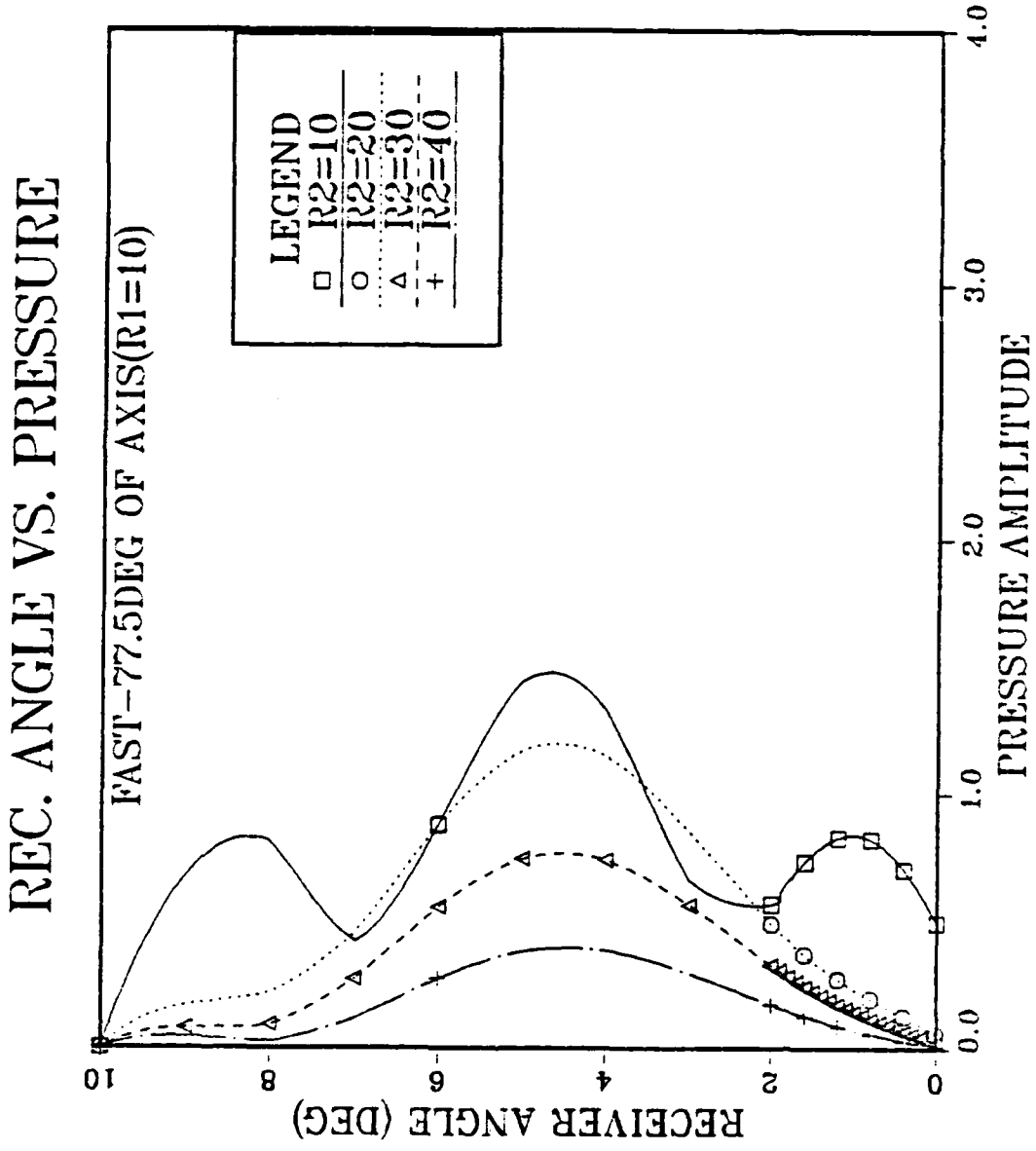

Figure 33. **Pressure Amplitude at 77.5° of Axis for Various R2 (R1=10) Over a Fast Bottom. (For clarity only every 5th computation shown)**

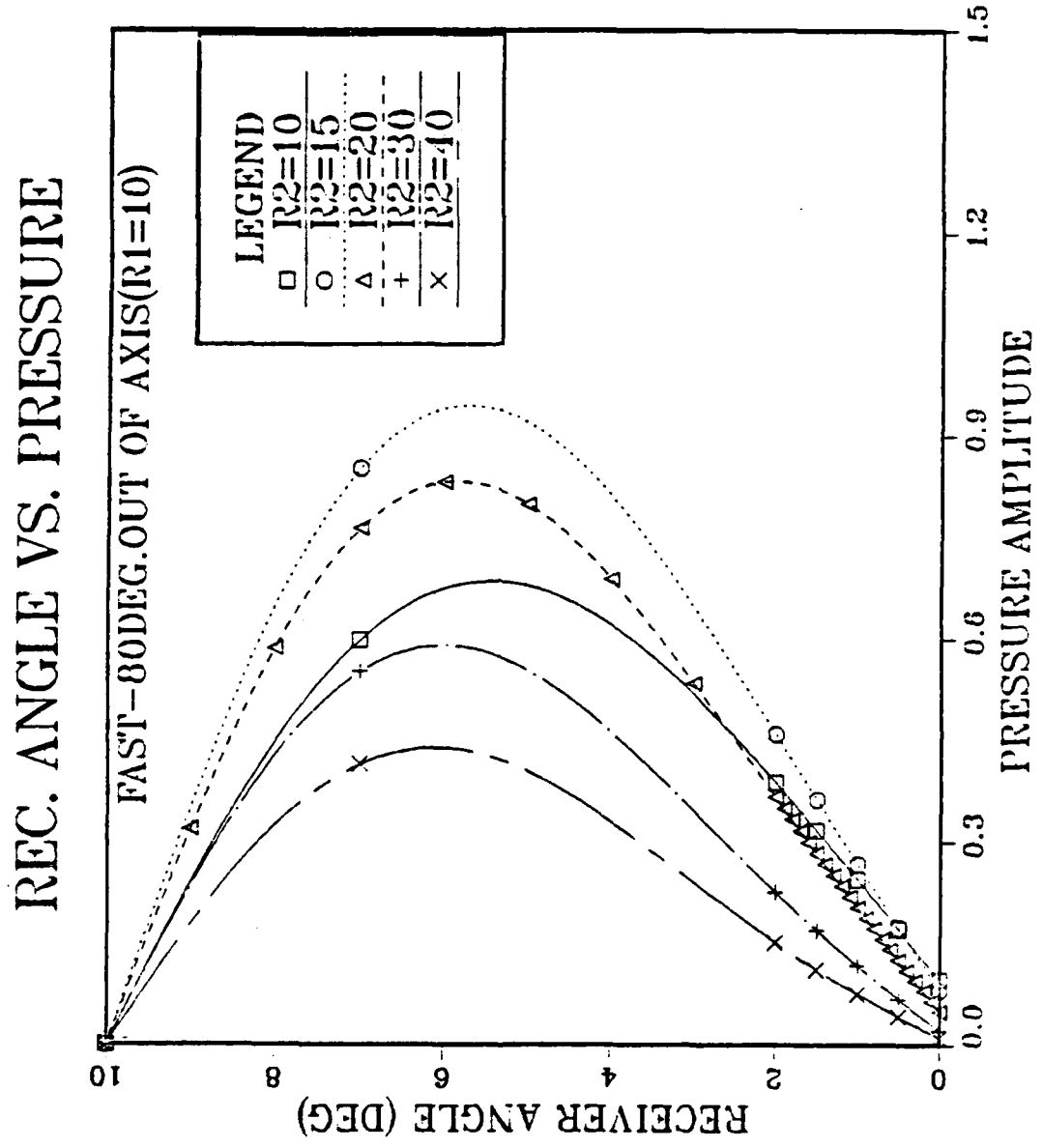

Figure 34. **Pressure Amplitude at 80° of Axis for Various R2 (R1=10) Over a Fast bottom. (For clarity only every 5th computation shown)**

APPENDIX C
DEME PROGRAM

= =

This program calculates the pressure amplitude and phase everywhere within a wedge shape fluid overlying a penetrable bottom. It is a modified version of the DSLOW program, which was written by CASWANDI. It has been modified by LT.D.PALIATSOS on March 89. This program is working for fast or slow bottoms. The output data are given by a table or by a graph using DISSPLA.

* *

```
      INTEGER   A,I,I1,M,N,S1,S2,N1,J,K
      REAL*4       B,CC,C2,D,D1,D2,G,PI,P1,P2,Q1,R1,R2,T,
     *           T4,T6,W0,W1,Y0,Y1,Y2,Z1,Z2,Z3,Z4,Z5,Z6,
     *           T1(80),R8(80),R9(80),S(30),C(30),E(30),
     *           F(30),Y,Z,R3,AL,PZ(30),DZ(30),V,DX,XP,DD,PN(30)
      REAL*4 TQQ,TQQ1,TQQ2,TQQ3
      PI =ACOS(-1.0D00)
C*********************************************************************
C     INPUT PARAMETERS
C*********************************************************************
C     B = WEDGE ANGLE (DEG)
C     G = SOURCE ANGLE (DEG)
C     D = RECEIVER ANGLE (DEG)
C     N1= # OF IMAGE POINTS
C     R1 = SOURCE DISTANCE (IN DUMP DISTANCES)
C     R2 = RECEIVER DISTANCE (IN DUMP DISTANCES)
C     Y0 = APEX DISTANCE (IN DUMP DISTANCES)
C     D1 = RHO 1/RHO 2
C     CC = C-1/C-2
C     AL = ALPHA/K2
C     A  = # OF RECEIVER POSITIONS
C*********************************************************************
C     INITIAL INPUT  RELATIONS
C*********************************************************************
      B = 5.5
      G = 2.75
      D = 00.0
      R1 = 1.3
      R2 = 9.0
      Y0 = 2.0
      D1 = 0.80
C     DO 90  P = 1,4
C
C  YOU MUST GIVE THE INFORMATION ABOUT THE BOTTOM, THAT
C  MEANS YOU MUST CHOOSE SLOW OR FAST BOTTOM BY GIVING
C  SOME VALUE TO THE SPEED RATIO CC = C1/C2 .        ]
C
C  CC=C1/C2
```

```
      CC =1.1
      AL = 0.0001
      A = 10
C*************************************************************************
C                    MAIN PROGRAM
C*************************************************************************
      K = 0
      N1 = INT(180./B)
      T6 = 180./PI
      B = B/T6
      G = G/T6
      C2 = CC**2
      D2 = (Y0*Y0)+(R1*R1)+(R2*R2)
      R3 = 2.*R1*R2
C     T4 = PI/(2*TAN(ACOS(1/CC))*TAN(B))
      TQQ = TAN(B)
C-------------------------------------------------------------------
C  DECISION ABOUT SLOW OR FAST BOTTOM
C-------------------------------------------------------------------
      IF (CC.LT.1) THEN
        TQQ1 =ACOS(CC)
        TQQ2 = SIN(TQQ1)
C       T4 = PI/(2*SIN(ACOS(CC))*TAN(B))  ***** FAST CASE
      ELSE
        TQQ1 = ACOS(1/CC)
        TQQ2 = TAN(TQQ1)
C       T4 = PI/2*TAN(ACOS(1/CC))*TAN(B)  **** SLOW CASE
      ENDIF
C-------------------------------------------------------------------
      TQQ3 = 2.*TQQ2*TQQ
      T4 = PI/TQQ3
C     K1X= PI/(2*TQQ*TQQ2)
      D2 = Y0*Y0+R1*R1+R2*R2
      Q1 = 1/DSQRT(2.0D00)
C300  FORMAT(' NOP   ',7X,'THETA(N) ',7X,'IMGE SR R8  ',7X,
C     *    'IMGE SR R9 ')
C     WRITE (6,300)
 800  FORMAT(5X,'REC.POS',5X,' REC.ANGLE ',5X,'PRES.AMPLITUDE ',5X,
     *   'PHASE ANGLE ',5X,'NORM.PRESS')
      WRITE (6,800)
      DO 10  M = 0,A
        D = M*B/A
        DD=B/A
        V =2*B/10
        IF(D.LT.V) GOTO 110
        IF(D.GE.V) GOTO 120
110     DX = D
      DO 15  J = 1,10
        D  = DX+(J-1)*B/(10*A)
        DD = B/(10*A)
 120    S1 = 1.0
```

```
      DO 20  N = 1,N1
       IF(S1.GT.0) T1(N)=(N-1)*B+G
       IF(S1.LT.0) T1(N)=N*B-G
       S1 = - S1
       R8(N) = SQRT(D2-R3*COS(T1(N)-D))
       R9(N) = SQRT(D2-R3*COS(T1(N)+D))
C310  FORMAT(3X,I2  ,5X,F5.2,4X,F6.4,6X,F6.4)
C     WRITE (6,310) N,T1(N),R8(N),R9(N)
 20   CONTINUE
      P1 = 0.0
      P2 = 0.0
      DO 30  N = 1,N1
       S2 = (-1)**(INT(N/2))
       W1 = 2*C2*AL
       I1 = INT((N-1)/2)
       DO 40  I = 1,I1
        S(I) = ABS(R1*SIN(T1(N)-2*I*B)
     *          +R2*SIN(2*I*B-D))/R8(N)
        C(I) = SQRT(1-(S(I)*S(I)))
        T = S(I)/D1
        W0 = (-C2+(C(I)*C(I)))
        Y = SQRT((W0*W0)+(W1*W1))
        Z =ABS(W0)
        IF(Y.LE.Z) Y = Z
        Y1 = Q1*SQRT(Y+W0)
        Y2 = -Q1*SQRT(Y-W0)
        Z1 = T-Y2
        Z2 = -Y1
C        Z12= CMPLX(Z1R,Z2I)
        Z3 = Z1/(Z1*Z1+Z2*Z2)
        Z4 =-Z2/(Z1*Z1+Z2*Z2)
        Z1 = T+Y2
        Z2 = Y1
C        Z13= CMPLX(Z3R,Z4I)
        Z5 = Z1*Z3-Z2*Z4
        Z6 = Z1*Z4+Z2*Z3
C        Z14= CMPLX(Z5R,Z6I)
        E(I) = Z5
        F(I) = Z6
C400  FORMAT(' NOP  ',5X,'I ',5X,'ARSIN(S(I)*T6)',5X,'E(I)',
C    *    5X,'F(I)',5X,
C    *     ' DSQRT(E(I)*E(I)+F(I)*F(I))',5X,'T6*ATAN(F(I)/E(I))')
C     WRITE (6,400)
C420  FORMAT(3X,I2.6X,I2,5X,F6.4,10X,F6.4,3X,F6.4,3X,F6.4,10X,F7.4)
C     WRITE (6,420) N,I, ASIN(S(I))*T6,E(I),F(I),
C    *          SQRT(E(I)*E(I)+F(I)*F(I)),ATAN(F(I)/E(I))
  40 CONTINUE
        Z1 = 0
        Z2 = 0
        Z3 = 0
        Z4 = 0
```

```
      Z5 = 1
      Z6 = 0
     IF(N.LE.2.00) GOTO 50
     DO 45  I = 1, I1
      Z1 = E(I)
      Z2 = F(I)
      Z3 = Z5
      Z4 = Z6
      Z5 = Z1*Z3-Z2*Z4
      Z6 = Z1*Z4+Z2*Z3
45  CONTINUE
50     Z1 = Z5
      Z2 = Z6
      T  = T4*R8(N)
      Z3 = COS(T)
      Z4 = -SIN(T)
      Z5 = Z1*Z3-Z2*Z4
      Z6 = Z1*Z4+Z2*Z3
      P1 = P1+S2*Z5/R8(N)
      P2 = P2+S2*Z6/R8(N)
C500  FORMAT(' NO.OF I.P ',3X,'RE(REFL)= ',3X,'IM(REFL)= ')
C     WRITE (6,500)
C510  FORMAT(3X,I2,6X,F6.4,6X,F6.4)
C     WRITE (6,510) N,S2*Z1,S2*Z2
C600  FORMAT(' I',5X,'ARCSIN(S(I))*T6=',3X,'E(I)',5X,'F(I)',5X.'EF',
C    *       5X,' AN2 ')
C     WRITE (6,600)
      I1=I1+1
    DO 60 I = 1, I1
      S(I) = ABS(R1*SIN(T1(N)-2*(I-1)*B)
     *          + R2*SIN(2*(I-1)*B+D))/R9(N)
      C(I) = SQRT(1-S(I)*S(I))
      T = S(I)/D1
      W0 = -C2+C(I)*C(I)
      Y = SQRT((W0*W0)+(W1*W1))
      Z = ABS(W0)
      IF(Y.LE.Z) Y = Z
      Y1 = Q1*SQRT(Y+W0)
      Y2 = -Q1*SQRT(Y-W0)
      Z1 = T-Y2
      Z2 = -Y1
      Z3 = Z1/(Z1*Z1+Z2*Z2)
      Z4 = - Z2/(Z1*Z1+Z2*Z2)
      Z1 = T+Y2
      Z2 = Y1
      Z5 = Z1*Z3-Z2*Z4
      Z6 = Z1*Z4+Z2*Z3
      E(I) = Z5
      F(I) = Z6
      AN1= ASIN(S(I))*T6
      EF = SQRT(E(I)*E(I)+F(I)*F(I))
```

```
      AN2= ATAN(F(I)/E(I))*T6
C610  FORMAT(2X,I2,5X,F6.4,5X,F6.4,5X,F6.4,5X,F6.4,5X,F7.4)
C     WRITE (6,610) I,AN1,E(I),F(I),EF,AN2
   60 CONTINUE
      Z1 = 0
      Z2 = 0
      Z3 = 0
      Z4 = 0
      Z5 = 1
      Z6 = 0
     DO 80 I = 1,I1
      Z1 = E(I)
      Z2 = F(I)
      Z3 = Z5
      Z4 = Z6
      Z5 = Z1*Z3-Z2*Z4
      Z6 = Z1*Z4+Z2*Z3
   80 CONTINUE
      Z1 = Z5
      Z2 = Z6
      T  = T4*R9(N)
      Z3 = COS(T)
      Z4 = -SIN(T)
      Z5 = Z1*Z3-Z2*Z4
      Z6 = Z1*Z4+Z2*Z3
      P1 = P1+S2*Z5/R9(N)
      P2 = P2+S2*Z6/R9(N)
C700  FORMAT(' LOWER PATH NO=',3X,'RE(REFL)= ',3X,'IM(REFL)= ')
C     WRITE ( 6,700)
C710  FORMAT(6X,I2,12X,F6.4,12X,F6.4)
C     WRITE (6,710) N,S2*Z1,S2*Z2
   30 CONTINUE
     K=K+1
     DZ(K)=D*T6
     PZ(K)=SQRT(P1*P1+P2*P2)*R1
C    WRITE (6,810) K,DZ(K),PZ(K),ATAN(P2/P1),PN(K)
C810  FORMAT(6X,I3,11X,F5.2,12X,F7.4,12X,F7.4,10X,F7.4)
 15   CONTINUE
 10   CONTINUE
     DO 31 L=1,29
     XP=PZ(28)
     PN(L)=PZ(L)/XP
     WRITE (6,811) L,DZ(L),PZ(L),ATAN(P2/P1),PN(L)
 811  FORMAT(6X,I3,11X,F5.2,12X,F7.4,12X,F7.4,10X,F7.4)
 31   CONTINUE
C250  FORMAT(' WEDGE ANGLE =   ',F5.2,1X,' SOURCE ANGLE    ',F4.2.1X,
C     *      ' SOURCE DISTANCE=',F4.2,1X,'RECEIVER DISTANCE= ',F4.2,1X,
C     *      ' SHORE DISTANCE= ',F4.2)
```

```
C     WRITE (6,250) B*T6,G*T6,R1,R2,Y0
C270            FORMAT('      RHO1/RHO2=',F5.2,5X,'      C1/C2='.F5.2.5X.'
AlPHA/K2=',F8.4)
C     WRITE (6,270) D1,CC,AL
C     YO = YO+2
C     R2 = R2+2
C     R1 = R1+2
 90   CONTINUE
      B = B*T6
      G = G*T6
C     STOP
C     END
C*********************************************************************
C
C     A PROGRAM FOR PLOTTING BY TEK618  OR SHERPA
C*********************************************************************
      CALL MEDBUF
      CALL TEK618
C     CALL SHERPA('SLOWDEM1','A',3)
      CALL NOBRDR
      CALL PAGE(15.,12.)
C     CALL PAGE(8.5,11.)
      CALL HWROT('AUTO')
C     CALL AREA2D(09.,5.)
      CALL AREA2D(09.,7.)
C     CALL AREA2D(8.5,6)
C     CALL AREA2D(6.0,8.5)
      CALL HEIGHT(.2)
      CALL XNAME('NORM. PRESSURE AMPLITUDE$',24)
      CALL YNAME('RECEIVER ANGLE(DEG)$',19)
      CALL YTICKS(5)
      CALL XTICKS(5)
      CALL GRAF(0.,2.0 ,10.0,0.,1.0,6.0)
C     CALL GRAF(0.,1.0 ,05.0,0.,1.0,06.0)
      CALL DOT
C     CALL GRID(2.2)
      CALL HEADIN('REC.ANGLE VS. NORM.PRESSURE$',-100,1.8.1)
      CALL MESSAG('WEDGE ANGLE =$',100,8.,7.)
      CALL REALNO(B,2,10.2,7.)
      CALL MESSAG('RHO1/RHO2 =$',100,8.,6.5)
      CALL REALNO(D1,2,10.2,6.5)
      CALL MESSAG('C1/C2 =$',100,8.,6.0)
      CALL REALNO(CC,2,10.2,6.)
      CALL MESSAG('SOURCE ANGLE= $',100,8.,5.5)
      CALL REALNO(G,2,10.2,5.5)
      CALL MESSAG('SOURCE DIST.= $',100,8.,5.)
      CALL REALNO(R1,2,10.2,5.)
      CALL MESSAG('REC.DIST. = $',100,8.,4.5)
      CALL REALNO(R2,2,10.2,4.5)
      CALL MESSAG('SHORE DIST.= $',100,8.,4.)
      CALL REALNO(Y0,2,10.2,4.)
      CALL MESSAG('PRESS.AMPL.(X=1) = $',100,7.0.3.5)
```

```
CALL REALNO(XP,105,10.2,3.5)
CALL RESET('ALL')
CALL PARA3
CALL NOCHEK
CALL CURVE(PN,DZ,29,1)
CALL ENDPL(0)
CALL DONEPL
STOP
END
```

LIST OF REFERENCES

1. Bradley, D., and Hudimac,A.A., *The Propagation of Sound in a Wedge Shaped Shallow Water Duct.* pp.2–9, The Catholic University of America, 1970.

2. Kuznetsov, V.K., *Method of Virtual Sources in the Underwater–Acoustical Description of High–Frequency Sound Fields in a Wedge.* Soviet Physics Acoustics, 18, No 2, pp 223–228, OCT–DEC 1972.

3. Kuznetsov, V.K., *Emergence of Normal Modes propagating in a Wedge on a Half Space from the Former to the Latter.* Soviet Physics Acoustics, 19(3), pp 241–245, NOV–DEC 1973.

4. Pierce, A.D., *Extension of the Method of Normal Modes to Sound Propagation in an Almost–Stratified Medium.* Jour.Acoust.Soc.Am., 37, 1965.

5. Milder, D.M., *Ray and Wave Invariants for SOFAR Channel Propagation.* Jour. Acoust. Soc.Am., 46, p 1259, 1969.

6. Graves, R.D., Nagli, A., and Uberall, H., *Range–Dependent Normal Modes in Underwater Sound Propagation: Application to the Wedge–Shaped Ocean.* Jour.Acoust.Soc.Am., 58(6), pp.1171–1177, December 1975.

7. Coppens, A.B., Sanders, J.V., Ioannou, I., and Kawamura, W., *Programs for the Evaluation of the Acoustic Pressure Amplitude and Phase at the Bottom of a Wedge–Shaped Fluid Layer Overlaying a Fast Fluid Half Space.* Naval Postgraduate School Report 61–79–002,December 1978.

8. Rubano, L., *Acoustic Propagation in Shallow Water Over a Low Velocity Bottom.* Jour.Acoust.Soc.Am., 67(5), pp.1608–1613, May 1980.

9. Jensen, F.B., and Kuperman, W.A., *Sound Propagation in a Wedge–Shaped Ocean with a Penetrable Bottom.* Jour.Acoust.Soc.Am., 67(5), pp.1566, May 1980.

10. Pierce, A.D., *Guided Mode Disappearance During Upslope Propagation in Variable Depth Shallow Water Overlying a Fluid Bottom.* Jour.Acoust. Soc. Am., 72(2), pp.523–531, August 1982.

11. Arnold, J.M., and Felsen, L.B., *Rays and Local Modes in a Wedge–Shaped Ocean.* Jour.Acoust.Soc.Am., 73(4), pp.1105–1119, April 1983.

12. Coppens, A.B., Humphries, M.,and Sanders, J.V., *Propagation of sound out of a fluid wedge into an underlying fluid substrate of greater sound speed.* Jour.Acoust.Soc.Am., 76(5), pp 1456–1465, November 1984.

13. Baek, C.K., *The Acoustic Pressure in a Wedge–Shaped Water Layer Overlying a Fast Fluid Bottom.* M.S.Thesis, Naval Postgraduate School. Monterey, California, March 1984.

14. LeSesne, P.K., *Development of Computer Programs Using the Method of Images to Predict the Sound Field in a Wedge Overlying a Fast Fluid and Comparison with Laboratory Experiments.* M.S.Thesis, Naval Postgraduate School, Monterey, California, December 1984.

15. Borchardt, J.A., *Measurements of the Acoustic Pressure Everywhere Over a Modeled Continental Slope.* M.S.Thesis, Naval Postgraduate School, Monterey, California, December 1985.

16. Tindle, C.T., Hobaek, H., and Muir, T.G., *Downslope Propagation of Normal Modes in a Shallow Water Wedge.* Jour.Acoust.Soc.Am., 81(2), pp 275–286. February 1987.

17. Kaswandi, C., *Computerized Investigation Using the Method of Images to Predict the Sound Field in a Fluid Wedge Overlying a Slow Fluid Half Space.* M.S.Thesis, Naval Postgraduate School, Monterey,California,1987.

18. Li Yu Ming, *Acoustic Pressure Distribution on the Bottom of a Wedge–Shaped Ocean.* M.S.Thesis, Naval Postgraduate School, Monterey. California, December 1987.

19. Doolittle, R, Tolstoy, A., and Buckingham, M., *Experimental Confirmation of Horizontal Refraction of CW Acoustic Radiation from a Point Source in a Wedge–shaped Ocean Environment.* Jour.Acoust.Soc.Am., 83(6), pp 2117–2125, June 1988.

20. Kinsler, Frey, Coppens and Sanders, *Fundamentals of Acoustics.* John Wiley & Sons, Third Edition, 1982.

21. Brekhovskikh, L.M., *Waves in Layered Media.* P.18, Academic Press, 1960.

22. Tolstoy I., and Biot M.A., *Formulation of Wave Propagation in Infinite Media by Normal Coordinates with an Application to Diffraction.* Jour.Acoust.Soc.Am., 29(3), pp.3870, 1956.

23. Personal Communication with A.B. Coppens and J.V.Sanders. Naval Postgraduate School, Monterey, CA 93940, March 1989.

INITIAL DISTRIBUTION LIST

1.	Defense Technical Information Center Cameron Station Alexandria,Virginia 22304–6145	2
2.	Library, Code 0142 Naval Postgraduate School Monterey, California 93943–5002	2
3.	Department Library, Code 61 Department of Physics and Chemistry Naval Postgraduate School Monterey, California 93943–5002	2
4.	Dr. A. B. Coppens, Code 61Cz Department of Physics and Chemistry Naval Postgraduate School Monterey, California 93943–5002	2
5.	Dr. J. V. Sanders, Code 61Sd Department of Physics and Chemistry Naval Postgraduate School Monterey, California 93943–5002	2
6.	Dr. A.A.Atchley, Code 61Ay Chairman, Acoustics Academic Committee Naval Postgraduate School Monterey, California 93943–5002	1
7.	Hellenic Navy General Staff Second Branch. Education Department Stratopedon Papagou Athens, GREECE	4
8.	LT. Demetrios Paliatsos H.N. 40 Ekklision 2 Bironas,16231 Athens,GREECE	4
9.	A. Tolstoy Acoustics Division, Code 5120.Naval Research Lab Washington DC 20375–5000	1

10. M. Buckingham 1
Royal Aircraft Establishment, Farnborough
Hampshire GU146TD, United Kingdom

11. Rad. Fountoulakis 1
58 Tanglewood Ln.
Monterey, CA 93940